Published in final edited form as:
Cell Chem Biol. 2021 August 19; 28(8): 1169–1179.e6. doi:10.1016/j.chembiol.2021.01.008.

Fatty acid chain length drives lysophosphatidylserine dependent immunological outputs

Neha Khandelwal[#1], **Minhaj Shaikh**[#2], **Amol Mhetre**[#1,*], **Shubham Singh**[#1], **Theja Sajeevan**[1], **Alaumy Joshi**[1,4], **Kithiganahalli Narayanswamy Balaji**[3], **Harinath Chakrapani**[2,*], **Siddhesh S. Kamat**[1,6,*]

[1]Department of Biology, Indian Institute of Science Education and Research (IISER) Pune, Dr. Homi Bhabha Road, Pashan, Pune 411008, Maharashtra, India

[2]Department of Chemistry, Indian Institute of Science Education and Research (IISER) Pune, Dr. Homi Bhabha Road, Pashan, Pune 411008, Maharashtra, India

[3]Department of Microbiology and Cell Biology, Indian Institute of Science (IISc), Bangalore 560012, Karnataka, India

[#] These authors contributed equally to this work.

Summary

In humans, lysophosphatidylserines (lyso-PSs) are potent lipid regulators of important immunological processes. Given their structural diversity and commercial paucity, here, we report the synthesis of methyl-esters of lyso-PS (Me-lyso-PS), containing medium to very-long chain (VLC) lipid tails. We show that Me-lyso-PSs are excellent substrates for the lyso-PS lipase ABHD12, and that these synthetic lipids are acted upon by cellular carboxylesterases to produce lyso-PSs. Next, in macrophages, we demonstrate that VLC lyso-PSs orchestrate pro-inflammatory responses and in turn neuroinflammation via a Toll-like receptor 2 (TLR2) dependent pathway. We also show that long chain (LC) lyso-PSs robustly induce intracellular cyclic AMP production, cytosolic calcium influx, and phosphorylation of the nodal extracellular signal-regulated kinase (ERK) to regulate macrophage activation via a TLR2-independent pathway. Finally, we report that LC lyso-PSs potently elicit histamine release during the mast cell degranulation process, and that ABHD12 is the major lyso-PS lipase in these immune cells.

Introduction

Lipids have long been known as potent signaling molecules that mediate many important physiological processes in mammals, including humans (Wymann and Schneiter, 2008, Dennis, 2016, Fahy et al., 2005). Prominent amongst the signaling lipids are the

[*]Correspondence to: siddhesh@iiserpune.ac.in; harinath@iiserpune.ac.in; amol@iiserpune.ac.in.
[4]Present address: Department of Biochemistry & Biophysics, Texas A&M University, College Station, Texas 77843, USA
[6]Lead contact

Author Contributions. N.K., S.S., T.S., and A.J. performed all the biochemical studies. M.S. and A. M. synthesized and characterized all the compounds; A.M. and H.C. supervised the synthesis. K.N.B. provided the TLR2 knockout mice for this study. S.S.K. conceived the project, acquired funding and wrote the paper with inputs from all authors.

Declaration of Interests. The authors declare no competing interests.

Europe PMC Funders Author Manuscripts

prostaglandins (Dennis and Norris, 2015), the endocannabinoids (2-arachidonoylglycerol (2-AG) and anandamide (AEA)) (Blankman and Cravatt, 2013, Fowler et al., 2005), and the well-studied lysophospholipids, sphingosine 1-phosphate (S1P) (Gonzalez-Cabrera et al., 2014, Rosen et al., 2013) and lysophosphatidic acid (lyso-PA) (Ishii et al., 2004, Contos et al., 2000). Given their physiological importance, the biosynthetic/degradative enzyme(s) and/or cognate receptor(s) of the aforementioned lysophospholipids (S1P and lyso-PA) are pharmacological targets for drugs already in clinical use or under investigations in different phases of clinical trials for an array of human neurological and immunological disorders (Gardell et al., 2006, Yanagida and Valentine, 2020). Recently, the lysophosphatidylserines (lyso-PSs) have emerged as yet another important class of signaling lysophospholipids (Shanbhag et al., 2020), with potent bioactivities in the mammalian central nervous and immune system.

Cellular pharmacological studies have shown that lyso-PSs regulate several immunological processes (Shanbhag et al., 2020) like macrophage activation to clear apoptotic cells (Frasch and Bratton, 2012), mast cell degranulation (Lloret and Moreno, 1995), leukemic cell stimulation (Park et al., 2005), chemotaxis of human gliomas (Lee et al., 2008), and maturation of regulatory T-cells (Barnes et al., 2015), and perhaps signal through Toll-like receptors (van der Kleij et al., 2002) and/or G-Protein coupled receptors (GPCRs) (Inoue et al., 2012) in the mammalian nervous and immune system. Interestingly, and of biomedical relevance, mutations to the putative lyso-PS receptors in humans, have been linked to different autoimmune diseases (Szymanski et al., 2014, Napier et al., 2015, Napier et al., 2014, Chu et al., 2013). Murine studies have recently shown that accumulation of lyso-PS, especially very long chain (VLC) lyso-PSs (Blankman et al., 2013), in the mammalian brain, is a major cause that drives the pathology of the early onset human neurological disorder PHARC (***p***olyneuropathy, ***h***earing loss, ***a***taxia, ***r***etinitis pigmentosa, and ***c***ataract) (Fiskerstrand et al., 2010, Fiskerstrand et al., 2009). Interestingly, PHARC is caused by deleterious mutations to the *abhd12* gene (Fiskerstrand et al., 2010, Fiskerstrand et al., 2009), that encodes an integral membrane metabolic serine hydrolase ABHD12 (**α**/**β** **h**ydrolase **d**omain containing protein # 12), a major, and to date, only *in vivo* functionally characterized lyso-PS lipase (Kamat et al., 2015, Blankman et al., 2013, Singh et al., 2020).

Given the strong link between lyso-PSs and human diseases, mechanistic studies are much needed to understand in more detail and biochemically characterize the signaling pathways influenced by lyso-PSs *in vivo*. The two factors complicating and/or limiting such studies are: (i) Unlike other signaling lipids (e.g. S1P, 2-AG, AEA), *in vivo* lyso-PSs are found esterified with different fatty acids (ranging from medium (C10) to VLC (C24)) (Blankman et al., 2013, Barnes et al., 2015), and hence, the precise physiological contributions of the individual lyso-PSs remain cryptic; (ii) Commercially, lyso-PSs are limited, and even those that are available, are esterified only with long chain (LC) fatty acids (C16:0, C18:0 and C18:1) (Figure 1A). Therefore, delineating the biological contributions of medium or VLC lyso-PSs has not been possible to date.

To address the aforementioned problems, here, we describe the synthesis of methyl-esters of lyso-PS (Me-lyso-PS) bearing fatty acids of varying chain lengths ranging from medium (C10 – C14) to LC (C16 – C20) to VLC (> C20) having the canonical natural (*R*)-

or unnatural (*S*)-configuration at the glycerol backbone. Next, we test these synthetic Me-lyso-PS lipids in a variety of biological assays, and show that the canonical (*R*)-Me-lyso-PSs are highly bioactive, while the corresponding unnatural (*S*)-Me-lyso-PSs are largely inactive. Specifically, we show that (*R*)-Me-lyso-PS are excellent substrates for the PHARC-associated lyso-PS lipase ABHD12, and confirm this enzyme's preference for VLC lyso-PS lipids (Joshi et al., 2018, Kamat et al., 2015, Blankman et al., 2013). Further, we show that cellular carboxylesterases hydrolyze the methyl-ester moiety of Me-lyso-PSs to yield lyso-PSs, and thus demonstrate that the synthetic Me-lyso-PSs serve as stable prodrug like biological precursors to lyso-PSs. Of note, we are the first to report, the distinct contribution of individual lyso-PS lipids in activation and pro-inflammatory responses from macrophages, and in the release of histamine during mast cell degranulation. Specifically, and of physiological importance, we show how the fatty acid chain length of lyso-PSs plays a critical role in the output of the aforementioned important immunological processes. Finally, we also annotate the metabolic serine hydrolase ABHD12 as a major lyso-PS lipase in primary mast cells, and expand the possible role of this biomedically important lipase to an additional immunological process.

Star Methods

Key Resource Table

Reagent or Resource Resource	Source	Identifier
Antibodies		
Rabbit, anti-phospho-p44/42 MAPK (ERK1/2) (20G11)	Cell Signaling Technology	Clone: monoclonal, catalog# 4376, RRID: AB_331772
Rabbit, anti-p44/42 MAPK (ERK1/2) (137F5)	Cell Signaling Technology	Clone: monoclonal, catalog# 4695, RRID: AB_390779
Rabbit, anti-GAPDH (EPR16891)	Abcam	Clone: monoclonal, catalog# ab181602, RRID: AB_2630358
Rabbit, anti-ABHD12 (EPR13683-72) (produced recombinantly, animal free)	Abcam	Clone: monoclonal, catalog# ab182011, RRID: Not available
Rabbit, anti-Iba1 (EPR16588)	Abcam	Clone: monoclonal, catalog# ab178846, RRID: AB_2636859
Rabbit, anti-beta actin	Cloud-Clone Corp.	Clone: polyclonal, catalog# CAB340Hu01, RRID: Not available
Rabbit, anti-TLR2	Novus Biologicals	Clone: polyclonal, catalog# NB100-56720, RRID: AB_838993
Goat, anti-rabbit IgG (H+L) secondary antibody, HRP conjugated	Thermo Fisher Scientific	Clone: polyclonal, catalog# 31460, RRID: AB_228341
Horse, anti-rabbit IgG (H+L) secondary antibody, Biotinylated	Vector Laboratories	Clone: polyclonal, catalog# BP-1100, RRID: Not available
ELISA Kits		
Mouse TNF-alpha DuoSet	R&D Systems	Catalog# DY410
Mouse IL-6 DuoSet	R&D Systems	Catalog# DY406
Human TNF-alpha DuoSet	R&D Systems	Catalog# DY210
Human IL-6 DuoSet	R&D Systems	Catalog# DY206
cAMP assay kit (competitive ELISA)	Abcam	Catalog# ab65355

Europe PMC Funders Author Manuscripts

Reagent or Resource Resource	Source	Identifier
Flou-8 calcium assay kit – medium removal	Abcam	Catalog# ab112128
ERK1 (pT202/pY204) + ERK2 (pT185/ pY187) + total ERK1/2 ELISA kit	Abcam	Catalog# ab126445
Chemicals, Peptides and Recombinant Proteins		
C16:0 Lyso-PS	Avanti Polar Lipids	Catalog# 858142
C18:0 Lyso-PS	Avanti Polar Lipids	Catalog# 858144
C18:1 Lyso-PS	Avanti Polar Lipids	Catalog# 858143
C17:1 Lyso-PS	Avanti Polar Lipids	Catalog# 858141
C18:0 Lyso-PA	Avanti Polar Lipids	Catalog# 857128
C18:0 Lyso-PG	Avanti Polar Lipids	Catalog# 858124
C18:0 Lyso-PC	Avanti Polar Lipids	Catalog# 855775
cis-10-Heptadecenoic acid (C17:1 FFA)	Sigma-Aldrich (Merck)	Catalog# H8896
Stearic acid	Sigma-Aldrich (Merck)	Catalog# S4751
Thioglycollate medium	Sigma-Aldrich (Merck)	Catalog# T9032
Lipopolysaccharide	Sigma-Aldrich (Merck)	Catalog# L3024
Mouse interleukin-3	Sigma-Aldrich (Merck)	Catalog# l4144
Mouse stem cell factor	Sigma-Aldrich (Merck)	Catalog# S9915
Sparstolonin B (SpaB)	Sigma-Aldrich (Merck)	Catalog# SML1767
Carboxylesterase from porcine liver	Sigma-Aldrich (Merck)	Catalog# 46058
Histamine	Sigma-Aldrich (Merck)	Catalog# H7125
Concanavalin A (Con-A)	Sigma-Aldrich (Merck)	Catalog# C0412
Polyethylenimine hydrochloride (PEI MAX®)	Polysciences	Catalog# 24765
Experimental Models: Organisms/Strains		
Mouse: C57BL/6J	The Jackson Laboratory	RRID: IMSR_JAX:000664
Mouse: ABHD12 null	Scripps Research	NA
Mouse: TLR2 null	The Jackson Laboratory	RRID: IMSR_JAX:004650
HEK293T cells	ATCC	CVCL_0063
THP-1 cells	ATCC	CVCL_0006
Software		
Prism 7 (version 7.0e)	GraphPad	https://www.graphpad.com/scientific-software/prism/
ImageJ v1.52u	NIH	https://imagej.nih.gov/ij/
SciexOS (version 1.4.0.18067)	Sciex	https://sciex.com/products/software/sciexos-software-x120805
Other		
Lipidomics data (mass spec)		Available from lead contact upon reasonable request

Results

Synthesis of Me-lyso-PS lipids

Structurally, lyso-PSs are composed of three building blocks: (i) a sugar backbone (glycerol), (ii) an amino acid head group (phospho-*L*-serine), and (iii) a lipid tail (fatty acid) (Figure 1A) (Fahy et al., 2011). It is this intricate combination of hydrophilic (glycerol and phospho-*L*-serine) and hydrophobic (fatty acid) biological building blocks that confers amphiphilic properties to lyso-PSs, and enables them to access different cellular membranes, organelles and compartments. Given this amphiphilic property, lyso-PSs serve as potent hormone-like mediators of various important immunological processes (Vance, 2015, Tracey et al., 2018, Shanbhag et al., 2020). From a stereochemical perspective, all natural lyso-PSs have two chiral centres: (i) α-carbon of the phospho-*L*-serine head group, and (ii) *sn-2* carbon of the (*R*)-glycerol backbone (Figure 1A) (Mallik et al., 2018). Biosynthetically, lyso-PSs are made from phosphatidylserine (PS) precursors, by the enzymatic action of PS-specific phospholipases (Hosono et al., 2001, Kamat et al., 2015), and subsequent studies have shown that physiologically, almost all lyso-PSs exists as 1-(fatty acyl)-2-hydroxy-*sn*-glycero-3-phospho-*L*-serine (Iwashita et al., 2009, Kamat et al., 2015). Given the synthetic challenges in making this bioactive lipid, for example, (i) combination of the aforementioned hydrophilic and hydrophobic moieties, (ii) lipophilicity of the final molecule, (iii) need for retention in configuration of the two chiral centres towards making the correct diastereomer, only three naturally occurring LC lyso-PSs (**1a-c**) are commercially available, thus limiting any rigorous structure activity relationship (SAR) studies for this important lysophospholipid class (Figure 1A). Since the commercial paucity of lyso-PSs would impede our proposed studies, here, we describe a facile synthesis route towards making Me-lyso-PS esterified with saturated fatty acids of varying chain lengths ranging from medium to VLC (Figure 1B, Supplementary Information). Speculating that the free reactive carboxylate moiety of the amino-acid end of the molecule might cross react and complicate the synthesis, we decided to make the Me-lyso-PS version. Our synthetic route, successfully afforded the naturally occurring canonical (*R*)-Me-lyso-PSs (Figure 1B, Supplementary Information) and the unnatural (*S*)-Me-lyso-PSs (Figure 1B, Supplementary Information) with same fatty acids (Figure 1B), to yield final compounds ((*R*)-**2a-h** or (*S*)-**2a-h**) in milligram quantities.

ABHD12 prefers VLC lyso-PSs as substrates

The lipids previously tested as substrates for the mammalian lyso-PS lipase ABHD12 have been, commercially available LC lyso-PSs (**1a-c**) (Blankman et al., 2013, Kamat et al., 2015) (Figure 1A), and various monoacylglycerol (MAG) lipids (Blankman et al., 2007, Joshi et al., 2018, Navia-Paldanius et al., 2012). In the absence of a commercial source for medium or VLC lyso-PSs, which to the best of our knowledge have not been tested against ABHD12, the MAG lipids have served as excellent surrogates for performing SAR studies towards biochemically understanding the substrate preference for this lipase (Joshi et al., 2018). Therefore, having synthesized the library of (*R*)- and (*S*)-Me-lyso-PSs containing medium, LC and VLC variants (nomenclature in Figure 1B), we first wanted to test if these lipids were indeed substrates for ABHD12. Leveraging established liquid-chromatography coupled to mass spectrometry (LC-MS) based substrate assays (Joshi et al., 2018), we found

that both recombinant human ABHD12 (hABHD12) (Table 1, Figure S1A) and endogenous mouse brain ABHD12 (mABHD12) (Figure S1B) robustly turned over (*R*)-Me-lyso-PSs, and for the same fatty acid, LC (*R*)-Me-lyso-PS and corresponding canonical natural LC lyso-PS behaved almost identically. Next, we performed rigorous enzyme kinetics measurements for our (*R*)-Me-lyso-PS library against hABHD12 (Figure 1C, Table 1), and found that, hABHD12 strongly prefers VLC (*R*)-Me-lyso-PSs as substrates with (*R*)-**2h** (C24:0, V_{max} = 22.9 ± 0.6 nmol/mg protein/min, *K*m = 40 ± 4 械 M), and (*R*)-**2g** (C22:0, V_{max} = 22.0 ± 0.6 nmol/mg protein/min, *K*m = 40 ± 4 械 M) being the best substrates. Further, mouse brain membrane lysates were assayed against the same Me-lyso-PS library, and here too, we found that mABHD12 strongly prefers VLC (*R*)-Me-lyso-PSs with (*R*)-**2h** (C24:0, Rate = 8.2 ± 0.3 nmol/mg protein/min), and (*R*)-**2g** (C22:0, Rate = 8.0 ± 0.3 nmol/mg protein/min) being the best substrates (Figure 1D). In this experiment, mouse brain membrane lysates from ABHD12-null mice were used as controls, to delineate specific contributions from mABHD12 (Figure 1D). In both these assays, we also tested (*S*)-Me-lyso-PSs, and found not surprisingly that, these were very poor substrates for hABHD12 (Table 1, Figure S1C) and mABHD12 (Figure S1D), with catalytic efficiencies 100-fold lower than that of corresponding (*R*)-Me-lyso-PSs for hABHD12 (Table 1). Taken together, these substrate assays conclusively show that the ABHD12 catalyzed lyso-PS lipase reaction is highly stereospecific, prefers VLC (*R*)-lyso-PSs as substrates, and, together with recent findings (Singh et al., 2020, Joshi et al., 2018), now provides a concrete biochemical explanation as to why VLC lyso-PSs accumulate the most in ABHD12 knockout mouse brains (Blankman et al., 2013).

Cellular carboxylesterases metabolize Me-lyso-PS to lyso-PS

Having synthesized Me-lyso-PSs, we postulated that these might be metabolized by cellular carboxylesterases to yield the corresponding lyso-PSs (Figure 2A). To test this hypothesis, we incubated three (*R*)-Me-lyso-PSs of varying lipid tails ((*R*)-**2b** (C12:0, medium chain) or (*R*)-**2e** (C18:0, LC) or (*R*)-**2b** (C24:0, VLC)) with active or denatured porcine liver carboxylesterase, and upon this treatment, by LC-MS (Joshi et al., 2018), we checked for the formation of the corresponding canonical lyso-PSs. We found for all the three (*R*)-Me-lyso-PSs subjected to this treatment, that upon incubation with active, but not the denatured carboxylesterase, the (*R*)-Me-lyso-PS was completely consumed, and a new peak was observed with mass shift of ~ 14 Da (parent m/z – 14 Da) (Figure 2A). The mass of this new peak corresponds to the loss of the methyl group from (*R*)-Me-lyso-PS to yield the corresponding canonical (*R*)-lyso-PS via hydrolysis by the carboxylesterase (Figure 2A). Since we planned to test this synthetic Me-lyso-PS library for different biological activities in mammalian macrophages and mast cells, we decided to test if lysates of these immune cells had carboxylesterases capable of converting (*R*)-Me-lyso-PS to the canonical lyso-PS lipid. To negate any lyso-PS lipase type activity, we used active or denatured lysates from ABHD12-null primary peritoneal macrophages or peritoneal-derived cultured mast cells, and found that the active, but not denatured lysates from both these immune cells, converted the three previously tested (*R*)-Me-lyso-PSs namely, (*R*)-**2b** (C12:0, medium chain), (*R*)-**2e** (C18:0, LC) and (*R*)-**2h** (C24:0, VLC), to their corresponding canonical (*R*)-lyso-PS lipid (Figure S2A). Our results clearly show that cellular carboxylesterases can hydrolyze the methyl group of (*R*)-Me-lyso-PSs to yield the corresponding canonical (*R*)-lyso-PSs (Figure

Europe PMC Funders Author Manuscripts

2A), and that the synthetic Me-lyso-PSs serve as stable prodrug-like biological surrogates to lyso-PSs, making them amenable to testing in primary macrophages and mast cells.

VLC lyso-PSs elicit robust pro-inflammatory responses in mammalian macrophages

Lyso-PSs have previously been shown to elicit immunological responses via pro-inflammatory cytokine secretion (e.g. TNF-α, IL-6) from mammalian macrophages (Kamat et al., 2015, Frasch and Bratton, 2012) and, we first wanted to assess if the Me-lyso-PSs were capable of the same, having shown that carboxylesterases in primary macrophages can metabolize Me-lyso-PSs to lyso-PSs (Figure S2A). We found that when primary peritoneal macrophages (PPM) isolated from wild type (WT) mice were treated with equal concentrations of the canonical LC lyso-PSs (**1a** (C16:0) and **1b** (C18:0)) and the corresponding (*R*)-Me-lyso-PSs ((*R*)-**2d** and (*R*)-**2e**) of the same lipid tail, they secreted almost equal amounts of pro-inflammatory cytokines (TNF-α, IL-6) (Figure S2B). Not surprisingly, treating PPM with unnatural (*S*)-Me-lyso-PSs (Figures S2C), corresponding free fatty acids (Figures S2C) or other lysophospholipids (lysophosphatidic acid (lyso-PA), lysophosphatidylglycerol (lyso-PG), and lysophosphatidylcholine (lyso-PC)) with same lipid tail (Figures S2D), failed to elicit any inflammatory response, suggesting that ligand recognition in PPM in eliciting pro-inflammatory responses is highly stereospecific for (*R*)-lyso-PSs. Having established comparable bioactivities of canonical lyso-PSs and (*R*)-Me-lyso-PSs, we isolated PPMs from WT or ABHD12 knockout mice, and incubated them with the (*R*)-Me-lyso-PS library to determine if the length of fatty acid tail had any effect of pro-inflammatory cytokine secretion. Interestingly, we found from this SAR study, that VLC (*R*)-Me-lyso-PSs, particularly (*R*)-**2g** (C22:0) and (*R*)-**2h** (C24:0), produced the highest pro-inflammatory cytokine secretion (TNF-α, IL-6) from WT PPM (Figure 2B). Not surprisingly, ABHD12-null PPM secreted significantly more pro-inflammatory cytokines compared to WT PPM upon (*R*)-Me-lyso-PS treatments, consistent with their diminished lyso-PS lipase activity (Kamat et al., 2015) (Figure 2B). For either genotype, the pharmacological Me-lyso-PS treatments did not have any effect on cell viability.

Here, we used the bacterial outer membrane glycolipid lipopolysaccharide (LPS) as a positive control, as this endotoxin tested in PPM mimics Gram-negative bacteria, and robustly elicits immunological responses (pro-inflammatory cytokine secretion) in PPM towards clearing this infection via a TLR4 dependent pathway (Raetz and Whitfield, 2002). In these assays, we found that the VLC (*R*)-Me-lyso-PSs treatments, produced ~ 60% pro-inflammatory cytokine secretion relative to similar LPS treatments in PPMs, suggesting that like LPS, VLC (*R*)-Me-lyso-PSs are potent immunological activators in mammalian macrophages (Figure 2B). We also performed a similar SAR study in human THP-1 macrophages, and found similar to results, that VLC (*R*)-Me-lyso-PSs produced the highest secretion of pro-inflammatory cytokines (Figure S2E).

VLC lyso-PSs signal via TLR2 in mammalian macrophages

Reported literature speculates that VLC lyso-PSs perhaps signal through Toll like receptor 2 (TLR2) (van der Kleij et al., 2002), though, to the best of our knowledge, VLC lyso-PSs have never been directly tested against any receptor for any immunological activity given their commercial unavailability. We found from a large-scale gene expression database

(Figure S3A) (Wu et al., 2016) and RT-PCR analysis (Figure S3B) that TLR2, but none of the other putative lyso-PS receptors (Inoue et al., 2012), is enriched on WT PPM. Consistent with literature precedence, we found that pharmacological antagonism of TLR2 using Sparstolonin B (SpaB) (Liang et al., 2011), ablated the increased pro-inflammatory cytokine secretion caused by VLC (*R*)-Me-lyso-PS treatments in WT PPM (Figure 3A), and in human THP-1 macrophages (Figure S2F). Here, we found that SpaB treatment also ablated the increased pro-inflammatory cytokine secretion caused by LPS treatment in WT PPM (Figure 3A), consistent with SpaB's dual TLR2/TLR4 antagonism activity (Liang et al., 2011, Liang et al., 2013). Next, we harvested PPM from TLR2 knockout mice (Figure S3C) (Holla et al., 2016), and measured pro-inflammatory cytokine secretion following (*R*)-Me-lyso-PS treatments. Consistent with the pharmacological studies, we found that VLC (*R*)-Me-lyso-PSs, particularly (*R*)-**2g** and (*R*)-**2h,** produced highest secretion of TNF-α and IL-6 from WT PPM, and this pro-inflammatory cytokine secretion was almost absent in TLR2-null PPM (Figure 3B).

ABHD12 knockout mice display increased cerebellar microgliosis, where the accumulation of VLC lyso-PSs speculatively causes this neuroinflammatory phenotype (Blankman et al., 2013). To test if VLC lyso-PSs indeed causes neuroinflammation, and if they signal through TLR2, we intravenously injected a VLC (*R*)-Me-lyso-PS ((*R*)-**2h,** C24:0) into WT or TLR2-null mice, and quantified the extent of neuroinflammation by counting the number of activated microglia using an established immunohistochemical protocol (Singh et al., 2020, Blankman et al., 2013). We find that systemic administration of (*R*)-**2h** (C24:0) robustly induced cerebellar microgliosis in WT, but not TLR2 knockout mice, suggesting that VLC (*R*)-Me-lyso-PSs signals through TLR2, causing neuroinflammation (Figures 3C, S4).

As a positive control, we used LPS (that signals through TLR4) (Raetz and Whitfield, 2002), and intravenously injected at the same dose and time, and found that the extent of neuroinflammation in WT and TLR2-null mice was almost the same (Figures 3C, S4). Further, we found that relative to the positive control LPS, the VLC (*R*)-Me-lyso-PS (*R*)-**2h** (C24:0) produced comparable neuroinflammation (Figures 3C, S4). Interestingly, a LC (*R*)-Me-lyso-PS ((*R*)-**2e**, C18:0) intravenous injection for the same dosing regime, did not produce any neuroinflammation in WT mice (Figure S4A, S4B). Taken together our results provide compelling *in vivo* evidence that, VLC lyso-PSs (but not LC lyso-PSs) signal through TLR2, elicit a robust pro-inflammatory immune response and are likely responsible for the neuroinflammation observed in ABHD12 knockout mice, the murine model of PHARC (Blankman et al., 2013).

Mammalian macrophages have a cryptic lyso-PS receptor

Mammalian macrophages in response to lyso-PS produce increased intracellular cyclic adenosine 5'-monophosphate (cAMP) (Sugita et al., 2013), cytosolic calcium (Ca^{2+}) influx (Park et al., 2005) and heightened phosphorylation of the nodal extracellular signal-regulated kinase (ERK) (Lee et al., 2008, Sugita et al., 2013), and we wanted to test if Me-lyso-PSs also produce these phenotypes in mammalian macrophages. We found in WT PPM that cellular cAMP (Figure 4A), relative cytosolic Ca^{2+} levels (Figure 4B),

and ERK phosphorylation (Figure 4C) increased most profoundly upon treatment with LC (*R*)-Me-lyso-PSs, especially (*R*)-**2e** (C18:0), and, that medium or VLC (*R*)-Me-lyso-PS had negligible effects on these phenotypes. Surprisingly, the genetic deletion of TLR2 in PPM (Figures S5A, S5B, S6C) or its pharmacological antagonism in PPM (Figures S5C, S5D, S6B) and human THP-1 macrophages (Figures S5E, S5F, S6B), showed no change on any of these phenotypes following (*R*)-Me-lyso-PS treatment. We also found that the LC (*R*)-Me-lyso-PSs (*R*)-**2e** (C18:0) and the corresponding canonical lyso-PS **1b** (C18:0) behaved identically in all these assays (Figures S6D, S6E, S6F). Not surprisingly, treating PPM with (*S*)-Me-lyso-PSs (Figures S6A, S6E, S6F), the corresponding free fatty acids or other lysophospholipids with lipid tail (C18:0) (Figures S6D, S6E, S6F), failed to elicit any significant response in any of these assays under similar treatment conditions, suggesting that these phenotypes in mammalian macrophages are specific to LC (*R*)-Me-lyso-PS (particular C18:0). In all these assays, we found that the pharmacological Me-lyso-PS treatments did not affect cell viability.

Of note, brains and LPS-treated PPM derived from ABHD12-null mice, (where, in absolute concentrations, **1b** (C18:0 lyso-PS) is the most abundant, and significantly deregulated lyso-PS (Blankman et al., 2013, Kamat et al., 2015)), have markedly more ERK phosphorylation compared to a WT control (Figure 4D). Given the heightened intracellular cAMP, cytosolic Ca^{2+} influx, phosphorylation of ERK, and inability of pharmacological antagonism or genetic disruption of TLR2 to affect any of these phenotypes, strongly supports the existence of another cryptic lyso-PS receptor on mammalian macrophages (in addition to TLR2) (Figure 4E). We speculate, based on aforementioned phenotypes, that this as-of-yet unknown receptor, is likely an unannotated GPCR (as putative lyso-PS GPCRs (Inoue et al., 2012) are absent in macrophages (Figure S3A, S3B)) that prefers LC lyso-PSs (particularly C18:0) as ligands, to produce its downstream biological effects (Figure 4E).

LC lyso-PSs robustly induce mast cell degranulation

The release of histamine during mast cell degranulation is the most investigated lyso-PS mediated immunological response (Sugo et al., 2006, Iwashita et al., 2009, Shanbhag et al., 2020), and yet contribution of individual lyso-PSs to this phenotype remain poorly understood. To address this, we generated peritoneal-derived cultured mast cells (PCMCs) (Meurer et al., 2016), and confirmed their ability to degranulate in presence of **1a** (C16:0 lyso-PS) or the corresponding (*R*)-Me-lyso-PS, (*R*)-**2d** (C16:0) in the presence of concanavalin A (Con-A) (Figure 5A) (Iwashita et al., 2009, Sugo et al., 2006). Con-A is a well characterized metalloprotein lectin of interest to immunologists, as it specifically binds mannosyl and/or glucosyl units of surface receptors of immune cells, and in doing so stabilizes receptor conformations, that in the context of PCMCs, facilitate antigen-dependent (lyso-PS) histamine release (Lawson et al., 1978, Sullivan et al., 1975). Having shown their ability to degranulate, we quantitatively measured the histamine release from PCMCs using an established LC-MS method (Chimalakonda et al., 2015) (Figure S7). Here, we found that the half-maximal effective concentration (EC_{50}) towards inducing histamine release during degranulation in PCMCs for **1a** (C16:0 lyso-PS, EC_{50} = 140 ± 22 nM) and (*R*)-**2d** (C16:0, EC_{50} = 179 ± 20 nM) were comparable, while the unnatural (*S*)-**2d** (C16:0, EC_{50} > 10 械 M) failed to produce this phenotype (Figure 5B), suggesting that the putative

receptor on PCMCs (likely GPR34 (Iwashita et al., 2009, Sugo et al., 2006), Figure S3A) is stereoselective in lyso-PS recognition. Next, we performed exhaustive dose response studies with the (*R*)-Me-lyso-PS library and found that (*R*)-**2d** (C16:0, EC_{50} = 179 ± 20 nM) most potently induced histamine release during PCMC degranulation, with other LC (*R*)-Me-lyso-PSs (*R*)-**2e** (C18:0, EC_{50} = 311 ± 37 nM) and (*R*)-**2c** (C14:0, EC_{50} = 645 ± 75 nM) following suite (Figure 5C). This SAR study showed that medium chain (< C12) or VLC (≥ C20) (*R*)-Me-lyso-PSs failed to induce PCMC degranulation (EC_{50} > 2.5 械 M) (Figure 5C), suggesting that besides the head group, the recognition of lipid tail, is another major factor contributing to histamine release from mast cells during degranulation. In this SAR study, we found that the pharmacological Me-lyso-PS treatments had no effect on cell viability.

ABHD12 is the major lyso-PS lipase in primary mast cells

ABHD12 is a major lyso-PS lipase in different immune cells (Ogasawara et al., 2018, Kamat et al., 2015), but its biochemical function in primary mast cells remains unknown. Western blot analysis (Figure 6A) and diminished lyso-PS lipase activity (Figure 6B) confirmed the loss of ABHD12 in PCMCs derived from ABHD12-null mice. We also found that ABHD12-null PCMCs secreted significantly more lyso-PS (~ 2-fold more **1a** (C16:0) and **1b** (C18:0)) compared to WT PCMCs (Figure 6C). Given the diminished lyso-PS lipase activity, we postulated that **1a** (C16:0 lyso-PS) treatment would cause ABHD12-null PCMCs to degranulate at a lower dose of **1a**, and thereby release histamine more efficiently than WT PCMCs. Indeed, ABHD12-null PCMCs (EC_{50} = 47 ± 17 nM) released histamine more effectively than WT PCMCs (EC_{50} = 135 ± 32 nM) upon similar **1a** (C16:0 lyso-PS) treatment (Figure 6D). Finally, we measured serum histamine concentrations following intravenous (*R*)-**2d** (C16:0) injection in WT or ABHD12 knockout mice, and found that ABHD12-null mice displayed heightened circulating histamine concentrations (~ 3-fold) compared to WT mice (Figure 6E). These results together confirm ABHD12's role as a major lyso-PS lipase in primary mast cells, where, by regulating serum lyso-PS levels (Figure 6E), it controls systemic histamine release (Figure 6E).

Discussion

Signaling lipids are potent hormone-like biological molecules which regulate several important physiological processes in mammals and their deregulation often has detrimental consequences that eventually manifests into disease in humans. Given their direct link to human diseases, the lyso-PSs have been recently emerged as another important class of signaling lipids (Shanbhag et al., 2020). However, unlike the established signaling lipids (e.g. 2-AG, AEA, S1P), *in vivo*, lyso-PSs exist esterified with different lipid tails ranging from medium chain (C10 – C14) to LC (C16 – C20) to VLC (> C20) fatty acids (Kamat et al., 2015, Blankman et al., 2013, Singh et al., 2020). Given the vast diversity in their *in vivo* content, it remains unclear as to which of these lyso-PSs have signaling functions, and how they influence, regulate and/or modulate different immunological processes. The lack of detailed SAR studies for these immunological phenotypes for lyso-PSs stems largely from the limited commercially availability, and reported synthetic strategies towards making them, especially the medium chain and VLC variants.

In this paper, we report the synthesis of Me-lyso-PSs having (*R*)- or (*S*)-stereochemistry at the *sn*-2 position of the glycerol backbone with varying lipid tails ranging from medium chain to LC to VLC (Figure 1, Supplementary Information). Since the synthesis of lyso-PSs has proved challenging, and that of VLC lyso-PSs has not been reported to be best of our knowledge, our synthetic strategy for the first time, allows performing rigorous SAR studies in diverse assays, to delineate the specific function of the lipid tail in modulating a phenotype regulated by lyso-PS. In all our biochemical and immunological assays, we find that (*R*)-Me-lyso-PSs serve as excellent bioequivalent surrogates for the canonical (*R*)-lyso-PSs, while the corresponding (*S*)-Me-lyso-PSs are biologically inactive. Since VLC lyso-PSs have never been tested against ABHD12, despite their accumulation in the brains of ABHD12-null mice (Blankman et al., 2013, Singh et al., 2020), here, by assaying the Me-lyso-PS library, we show conclusively that the ABHD12 catalyzed lyso-PS lipase reaction is stereoselective, and prefers VLC lyso-PSs are substrates (Figure 1). Further, we show using biochemical assays that, the (*R*)-Me-lyso-PSs are acted upon by cellular carboxylesterases, converted to the corresponding canonical (*R*)-lyso-PSs, and therefore biologically, the (*R*)-Me-lyso-PSs function as prodrug like surrogates for lyso-PS in primary macrophages and mast cells (Figure 2).

Next, we wanted to understand the distinct role that the lipid tail of individual lyso-PSs plays in the activation of macrophages and mast cell degranulation, as these immunological processes have been reported to be regulated by lyso-PSs (Shanbhag et al., 2020). In mammalian macrophages, we find that VLC Me-lyso-PSs produce the highest secretion of pro-inflammatory cytokines and that these pro-inflammatory responses are higher in ABHD12-null macrophages (Figure 2), given their diminished lyso-PS lipase activity (Kamat et al., 2015). Next, using pharmacological tools and genetic models, we show conclusively that VLC Me-lyso-PSs (but not LC lyso-PSs) orchestrate robust pro-inflammatory responses via a TLR2-dependent pathway to cause neuroinflammation (Figure 3). That VLC lyso-PSs signal through TLR2 and causes neuroinflammation (Figure 3, S4) raises an intriguing possibility, corroborating a recent report (Ogasawara et al., 2018), that the human neurological disease PHARC may itself be an autoimmune disease. Further, we find that mammalian macrophages produce increased intracellular cAMP, cytosolic Ca^{2+} flux and heightened ERK phosphorylation in response to LC lyso-PS treatments (particularly C18:0 lyso-PS) (Figure 4) via a TLR2-independent pathway (Figure S5, S6), and we speculate that there is another cryptic receptor, likely a GPCR, that prefers LC lyso-PSs (particularly C18:0 lyso-PS) as ligands to produce these biological activities (Figure 4). Next, we show that LC lyso-PSs (especially C16:0 lyso-PS), but not medium of VLC lyso-PSs, efficiently cause the release of histamine from mast cells during degranulation, and suggests that the putative lyso-PS receptor on mast cells (possibly GPR34 (Sugo et al., 2006)) prefers LC lyso-PSs (particularly C16:0 lyso-PS) as ligands to drive this immunological process (Figure 5). Finally, we report that ABHD12 is the major lyso-PS lipase in primary mast cells, where it controls the secreted lyso-PS levels and its deletion in mice, results in elevated levels of serum histamine and lyso-PS (Figure 6).

Projecting ahead, we propose that the functional antagonism of TLR2 might provide an excellent therapeutic paradigm in treating PHARC. This premise can be tested genetically by generating and characterizing ABHD12-TLR2 dual knockout mice, and

pharmacologically, by discovering much needed *in vivo* active TLR2 functional antagonists. Next, the annotation of ABHD12 as a major lyso-PS lipase in primary mast cells provides yet another avenue in understanding the immunomodulatory properties and the functional cross-talk of lyso-PSs between different immune cells particularly in the context of allergies and autoimmune conditions (Kelkar et al., 2019, Ogasawara et al., 2018). Finally, we would like to note that a major shortcoming of our study, is the inability of our synthetic strategy in making Me-lyso-PSs with unsaturated fatty acid chains. Therefore, the development of such a synthetic methodology, would enable making Me-lyso-PSs with unsaturated fatty acid chains, and can also be leveraged to generate lyso-PS probes with suitable recently reported biorthogonal handles (Niphakis et al., 2015). Such bifunctional lyso-PS probes in tandem with advanced mass spectrometry based chemoproteomics platforms (Niphakis et al., 2015, Parker et al., 2017) will greatly facilitate the identification of hitherto unknown lyso-PS protein ligands and/or receptors, and this new knowledge will certainly expand our biological understanding for this emerging immunomodulatory lipid class.

Significance

Lysophospholipids are potent hormone-like biological mediators that regulate many important physiological processes in mammals. Recently, the lysophosphatidylserines (lyso-PSs) have emerged as yet another class of signaling lysophospholipids, with potent bioactivities in the central nervous and immune system in mammals, and deregulation in their metabolism has been linked to neurological and autoimmune disorders in humans. However, challenges in making lyso-PSs synthetically, and limited commercial sources for this lipid class, have greatly hampered any exhaustive structure-activity relationship (SAR) studies, towards mechanistically understanding the role that lyso-PSs play in different physiological processes. Here, we report a facile synthetic strategy towards making methyl-esters of lyso-PSs (Me-lyso-PSs) with varying lipid tails, which serve as prodrug like biological surrogates for lyso-PSs, and focused on elucidating the role that lipid tail of this lysophospholipid plays in regulating various immunological processes. Specifically, we study the lyso-PS mediated activation of macrophages and mast cell degranulation processes, and show through detailed SAR studies, that lipid tail has profound effects on the phenotypical outputs of these important immunological processes. Our findings thus illuminate a physiological balance between long chain and very long chain lyso-PSs, intricately regulated by the lyso-PS lipase ABHD12, and disrupting this fine-tuned homeostasis results in immunological outputs, that have detrimental pathological consequences in humans.

Lead Contact and Materials Availability

Further information and materials request should be directed to the Lead Contact, Siddhesh S. Kamat (siddhesh@iiserpune.ac.in). This study has generated some unique compounds, and these can be made available from the Lead Contact with a completed Materials Transfer Agreement.

Experimental Model and Subject Details

Mice. All mouse studies and experiments described in this paper have received formal approval from the Indian Institute of Science Education and Research, Pune – Institutional Animal Ethics Committee (IISER-P IAEC) (application nos: IISER_Pune IAEC/2016_02/01, and IISER_Pune IAEC/2019_2/07) constituted as per the guidelines and norms provided by the Committee for the Purpose of Control and Supervision of Experiments in Animals (CPCSEA), Government of India. All experimental mice were housed in the National Facility for Gene Function in Health and Disease (NFGFHD), IISER Pune, and were studied between 2 – 6 months of age. All mice had *ab libitum* access to food and water. Thioglycollate elicited primary peritoneal macrophages (PPMs) (Kamat et al., 2015) and peritoneal-derived cultured mast cells (PCMCs) (Meurer et al., 2016) were generated from mice 10 – 12 weeks of age, and harvested from mice and cultured using established protocols. For all mouse experiments, equal number of male and female mice were used, and age/sex matched littermates were used as controls. All strains of mice used in this study as reported in the **Key Resource Table.**

Mammalian cell lines. HEK293T and THP-1 cells were purchased from the ATCC, and cultured in RPMI1640 medium supplemented with 10% (v/v) FBS and antibiotics (1% (v/v) penicillin-streptomycin (MP Biomedicals)) at 37 °C with 5% (v/v) CO_2. Cell staining with 4',6-diamidino-2-phenylindole (DAPI) was routinely performed to ensure that all cell lines were devoid of any mycoplasma contamination. All cell lines were grown to ~80% confluency, and all live cells were estimated on a TC20 automated cell counter using trypan blue reagent as per manufacturer's protocol (Bio-Rad).

Method Details

Reagents. Unless otherwise mentioned, all the following materials used in the experiments described in this paper were purchased from the commercial source mentioned in the parenthesis: chemicals, buffers and reagents (Sigma-Aldrich), commercial lipids and lipid standards (Avanti Polar Lipids), primary and secondary antibodies (Abcam), and tissue culture media and Fetal Bovine Serum (FBS) (HiMedia).

Lyso-PS lipase substrate assays. Wild type (WT) human ABHD12 (hABHD12) or the catalytically inactive active site mutant S246A hABHD12 were transiently transfected in HEK293T cells using a polyethylenimine-based (PEI MAX®) transfection methodology (Joshi et al., 2018, Kamat et al., 2015) along with mock (empty plasmid) controls, and the membrane lysates from these were prepared as reported earlier (Kelkar et al., 2019, Joshi et al., 2018). The brain membrane lysates from wild type and ABHD12 knockout mice were also prepared using a protocol reported earlier (Joshi et al., 2018, Singh et al., 2020). The lyso-PS lipase assays described in this paper were performed using an established LC-MS method that measures the release of free fatty acids from lyso-PS substrates by the lipase activity of ABHD12 relative to an unnatural fatty acid internal standard (C17:1 FFA, 0.5 nmol) (Joshi et al., 2018, Singh et al., 2020). All assays done using 10 械 g of HEK293T membrane lysates transfected with hABHD12 or 20 械 g of brain membrane lysates for 30 mins, as previous studies have shown that the lyso-PS lipase assay is linear for this

protein concentration and time over a range of substrate concentrations (Joshi et al., 2018). All single concentration lipase (substrate) assays were done using 100 械 M of the lipid substrate, while the enzyme kinetic studies were done over the concentration range of 0 – 400 械 M for the particular lipid that was assayed.

Mammalian cells lipid treatments. For the pro-inflammatory cytokine measurements, macrophages (1 x 10^6 PPMs or 0.5 x 10^6 THP-1 cells) were plated in 6-well plates (Eppendorf) in 2 mL of RPMI1640 media without any supplementation, and treated with vehicle (DMSO) or lipids [commercial lyso-PSs or (*R*)-Me-lyso-PSs or (*S*)-Me-lyso-PSs or free fatty acids, or other C18:0 lysophospholipids (lyso-PA, lyso-PG and lyso-PC)] or LPS (positive assay control) all at 1 械 M final concentration for 4 h at 37 °C. Following this treatment, the media (1.5 mL) was collected and stored at – 80 °C till the analysis was completed. The pro-inflammatory cytokines (TNF-α and IL-6) were quantitatively measured using standard single analyte ELISA assays as per manufacturer's instructions (R&D Systems). For the cellular cyclic adenosine 5'-monophosphate (cAMP), cytosolic calcium (Ca^{2+}) and ERK phosphorylation measurements, macrophages (4 x 10^6 PPMs or 2 x 10^6 THP-1 cells) were plated in 6-well plates (Eppendorf) in 3 mL of RPMI1640 media without any supplementation, and treated with vehicle (DMSO) or lipids [commercial lyso-PSs or (*R*)-Me-lyso-PSs or (*S*)-Me-lyso-PSs or free fatty acids, or other C18:0 lysophospholipids (lyso-PA, lyso-PG and lyso-PC)] or LPS (positive assay control) all at 1 械 M final concentration for 10 mins at 37 °C. Following this treatment, the assay plates were centrifuged at 1400g for 5 min to pellet the live cells, and separate the media. The media was removed by pipetting, following which, the cells were washed with sterile cold Dulbecco's phosphate buffer saline (DPBS) (x 3 times) at 4 °C, and lysed by sonication in 500 械 L cold sterile DPBS at 4 °C. The cell lysates were deproteinized by passing them through a 3000 (3-kDa) molecular weight filter, and the flow through was eventually used to estimate the cellular levels of cAMP and free cytosolic Ca^{2+}. For phosphorylated ERK measurements, total cell lysates without the deproteinization step were used. The changes (increase) in cellular cAMP, free cytosolic Ca^{2+} and ERK phosphorylation in response to the aforementioned treatments were quantitatively estimated using standard competitive ELISA based colorimetric (cAMP, ERK phosphorylation) and fluorometric (free cytosolic Ca^{2+}) assays as per manufacturer's instructions (Abcam). All pharmacological TLR2 antagonism studies (Liang et al., 2011, Liang et al., 2013) described in this paper, were done at 10 械 M final concentration of SpaB for 4 h at 37 °C.

Western blot analysis. Cell or tissue lysates were prepared as described earlier (Joshi et al., 2018), the protein concentrations from them were estimated using the Pierce BCA Protein Assay kit (Thermo Fisher Scientific), and the western blot analysis was done using previously reported protocols (Rajendran et al., 2020, Joshi et al., 2018). Briefly, 50 械 g protein lysate was resolved on a 12% SDS-PAGE gel and transferred onto a PVDF membrane (GE Healthcare) (60 mA, 12 h, 4 °C). Post-transfer, the membrane was blocked with 5% (w/v) skimmed milk in 1X phosphate buffered saline containing 0.1% (w/v) Tween-20 (PBST) (blocking buffer) for 1 h at room temperature (20 – 25 °C), washed with PBST (x 3 times) and subsequently probed with the primary antibody (dilution 1:1000) in blocking buffer for 12 – 14 h at 4 °C. Following this, the membrane was washed with PBST

(x 3 times), and incubated with a horse-radish peroxidase (HRP) conjugated anti-rabbit IgG (H + L) (goat, Thermo Fisher Scientific, 31460, 1:10,000) secondary antibody for 1 h at room temperature (20 – 25 °C). Finally, the membrane was washed with PBST (x 3 times), and the signal was visualized with SuperSignal West Pico Chemiluminescent substrate (Thermo Fisher Scientific) on a Syngene G-Box Chemi-XRQ gel documentation system. For the phosphoprotein immunoblotting, the cells and tissues were lysed in buffer containing phosphatase inhibitors (1 mM sodium orthovanadate, 1 mM sodium pyrophosphate, 5 mM sodium fluoride) to maintain intact protein phosphorylation at serine, threonine and/or tyrosine protein residues. A complete list of all the primary antibodies used in this study can be found in the **KEY RESOURCE TABLE**.

ELISA assays. All quantitative pro-inflammatory cytokine measurements (TNF-α, IL-6) were done using single analyte ELISA assays from R&D Systems as per manufacturer's instructions. For measuring intracellular cAMP, cytosolic free Ca^{2+} and phosphorylated ERK, ELISA kits were purchased from Abcam, and the assays were performed as per manufacturer's instructions. A complete list of all the ELISA kits used in this study can be found in the **KEY RESOURCE TABLE.**

RT-PCR. The total RNA was isolated from mouse PPM using the RiboZol™ RNA extraction reagent (Amresco), and the first strand cDNA was synthesized from the isolated total RNA using the ThermoScript™ RT-PCR System (Invitrogen) as per manufacturer's protocol. The primers listed below were used to yield the fragment size in parenthesis for the following gene products for the gel represented in Figure S3B:

GRP34: 5'-GAGCACTTCGGCTTACTTGG-3' and 5'-TTCCATGAGAGGAGCAAAGC-3' (422-bp); *GPR174*: 5'-CTGCATCAGTGTGCGAAGAT-3' and 5'-TCACTCTTCTGGCAAAGCAA-3' (479-bp); *P2Y10*: 5'-AAGAGCCCAGCTGACACAAC-3' and 5'-AAGAGCCCAGCTGACACAAC-3' (439-bp); *TLR2*: 5'-GACTCACAGCAGCCATGAAA-3' and 5'- TCGCGGATCGACTTTAGACT-3' (451-bp); *ACTB*: 5'-GGGAATGGGTCAGAAGGACT-3' and 5'-ACGCTCGGTCAGGATCTTC-3' (454-bp); *GAPDH*: 5'-ACTTGAAGGGTGGAGCCAAA-3' and 5'-AGATCCACGACGGACACATT-3' (403-bp).

Immunohistochemical analysis. The immunohistochemical analysis were done using a protocol recently published by us with minor modifications (Singh et al., 2020). Briefly, mice were deeply anaesthetized using isoflurane and perfused first with cold phosphate buffer saline (PBS), and then with 4% (w/v) paraformaldehyde (PFA) in PBS. Brains were dissected and post-fixed in 4% (w/v) PFA in PBS overnight at 4 °C and then transferred into 30% (w/v) sucrose in PBS until brains sank to bottom of the tubes (~ 3 days). Coronal 25 μm cerebellar sections were cut on a freezing microtome (Leica CM1950), maintained at – 30 °C and 1 out of every 6 sections was collected for assessing microglial activation. Endogenous peroxidases were inactivated with 3% (v/v) hydrogen peroxide in PBS for 15 min. Thereafter the sections were washed twice with 1% bovine serum albumin (BSA) (HiMedia) in PBS, and permeabilized with 0.1% (w/v) Triton-X 100 and 0.5% (w/v) BSA in PBS at room temperature (20 – 25 °C) for 45 mins. The sections were then incubated

with primary monoclonal anti-Iba1 antibody [rabbit, Abcam, Cat: ab178846, 1:1000] in 1% (w/v) BSA in PBS overnight at 4 °C. Following overnight incubation, the sections were washed three times with 0.5% (w/v) BSA in PBS and incubated with secondary antibody, biotinylated anti-rabbit [horse, Vector labs, BP-1100, 1:500] in 0.5% (w/v) BSA in PBS for 1 h at room temperature (20 – 25 °C). Following this treatment, the sections were washed twice in 0.5 % (w/v) BSA in PBS, incubated with ABC Elite Vectastatin (Vector labs, Cat: PK-6100) for 1 h at room temperature (20 – 25 °C) and subsequently washed twice with excess PBS. Finally, the sections were stained with Immpact DAB (Vector labs, Cat: SK-4105) for 3 min in the dark, transferred to excess PBS and mounted in VectaMount (Vector labs, Cat: H-5000) after drying. Activated microglial cells (area > 200 μm^2) in matching cerebellar sections were quantified using the ImageJ software (NIH) (Rueden et al., 2017, Schindelin et al., 2015) as per previously reported protocols (Blankman et al., 2013, Singh et al., 2020).

Histamine estimation from mast cells. The PCMCs were isolated from the peritoneal cavity of mice (10 -12 weeks of age) and cultured using a previously reported protocol (Meurer et al., 2016) with typical yields of ~ (1 x 10^6) PCMCs per mouse. To assess the extent of lyso-PS induced degranulation of PCMCs, histamine release from these cells was measured using an established LC-MS method (Chimalakonda et al., 2015), which we validated using an authentic histamine standard (Figure S7). Towards this, PCMCs were first pelleted (1400g for 5 min) and subsequently re-suspended in Hank's Balanced Salt Solution (HBSS) containing 1% (w/v) heat inactivated FBS at a concentration of 5 x 10^6 cells/mL. All assays were performed in a 96 well plates with "V" bottoms (Tarsons) to a final volume of 100 μL at 37 °C with 5% (v/v) CO_2. The vehicle (DMSO) or lipids (commercial lyso-PSs or (*R*)-Me-lyso-PSs or (*S*)-Me-lyso-PSs); ranging from 1 nM – 100 μM concentration in the assay) were added to individual wells with or without Con-A (1 mg/mL final assay concentration) to make volume to 90 μL in HBSS. To this, 10 μL of the PCMC cell stock (5 x 10^6 cells/mL) pre-incubated at 37 °C with 5% (v/v) CO_2 was added such that each assay well finally contained 5 x 10^3 cells, and the assay allowed to proceed for 30 mins at 37 °C with 5% (v/v) CO_2. At this point, to quench the assay, the cells were pelleted by centrifugation (1200g for 5 mins), and 50 μL of the media was collected for estimation of secreted histamine levels. To this 50 μL of media, 150 μL of LC-MS grade acetonitrile (Sigma-Aldrich) was added, the mixture was vortexed and stored at – 80 °C till the histamine estimations were performed by LC-MS. The pellet cells were re-suspended in the remaining 50 μL media by vigorous vortexing and lysed by sonication in a water bath at 37 °C. The cell lysates were then added to 150 μL of MS grade acetonitrile (Sigma-Aldrich), the mixture was vigorously vortexed and stored at – 80 °C till the histamine estimations were performed. The histamine release from PCMCs was calculated in accordance to a formula reported for this LC-MS method (Chimalakonda et al., 2015). For measuring circulating serum histamine concentrations, 1 volume of mouse serum (typically 200 – 300 μL) obtained from whole blood of wild type or ABHD12 knockout mice (12 – 14 weeks of age), was mixed with 2 volumes (400 – 600 μL) MS grade acetonitrile (Sigma-Aldrich), the mixture was centrifuged at 2000g for 5 mins to pellet the protein debris, and the supernatant was collected, dried, and re-suspended in 50 μL MS grade acetonitrile (Sigma-Aldrich), and assessed thereafter by LC-MS as per

a previously reported protocol (Chimalakonda et al., 2015). The quantitation for serum histamine levels, was done using a standard calibration curve for histamine (5 – 5000 ng/mL serum). All histamine measurements were done using an established LC-MS method (Chimalakonda et al., 2015) in the positive ion mode using high resolution multiple reaction monitoring (MRM-HR) analysis on a Sciex X500R quadrupole time-of flight (QTOF) mass spectrometer fitted with an Exion UHPLC system using a Kinetex 2.6 μ m HILIC column with 100 Å particle size, 150 mm length and 3 mm internal diameter (Phenomenex). The MRM-HR mass spectrometry parameters for measuring histamine are: precursor ion mass (Q1, $M+H^+$) = 112.0869, product ion mass (Q3, $M+H^+$) = 95.0604, declustering potential = 100 V, entrance potential= 10 V, collision energy = 50 V, and collision exit potential = 10 V. Complete details of the sensitivity and dynamic range of the LC-MS method for histamine estimation, and the co-elution studies with a histamine standard can be found in Figure S7.

Lyso-PS measurements. The organic extractions to enrich lyso-PS lipids, and all the LC-MS based quantitative lyso-PS measurements (secreted lyso-PS concentrations from PCMCs (Figure 6C), and the serum lyso-PS levels (Figure 6E)) were performed using an established and previously reported protocol (Kelkar et al., 2019, Singh et al., 2020, Pathak et al., 2018). The measurements of lyso-PS (product) formed following porcine liver carboxylesterase (0.1 U, 15 mins, 37 °C) or immune cell lysate (ABHD12-null PPM or PCMC, 20 μ g, 15 mins, 37 °C) treatment of Me-lyso-PS (100 μ g) was also done using the same reported protocols (Singh et al., 2020, Kelkar et al., 2019, Joshi et al., 2018).

Synthesis and compound characterization. Complete details of synthesis of all the compounds reported in this paper, their chemical/analytical characterization and all the spectral data associated with these compounds can be found in the Supplementary Information associated with this paper.

Quantification and Statistical Analysis

All data represented in this paper is shown as mean ± standard deviation unless otherwise mentioned. All statistical analyses were performed using the GraphPad Prism 7 (version 7.0e) software for Mac OS. The Student's two-tailed *t* test was used to determine the statistical significance between the different study group, and a *P* value of < 0.05 was considered statistical significant for all the assays reported in this study.

Supplementary Material

Refer to Web version on PubMed Central for supplementary material.

Acknowledgments

This work was supported by a DBT/Wellcome Trust India Alliance Fellowship (grant number IA/I/15/2/502058) awarded to S.S.K., a Department of Science and Technology (DST) Fund for Improvement of S&T Infrastructure (grant number SR/FST/LSII-043/2016 to IISER Pune Biology Department), and a J. C. Bose National Fellowship from the Science & Engineering Research Board (SERB), DST (SB/S2/JCB-025/2016 to K.N.B.). N.K. acknowledges a DST-SERB postdoctoral fellowship, and M.S. acknowledges a graduate student fellowship from the Council of Scientific and Industrial Research (CSIR). Benjamin F. Cravatt, The Scripps Research Institute is thanked for providing the ABHD12 knockout mice used in this study. The National Facility for Gene Function in Health and Disease (NFGFHD), IISER Pune (supported by a grant from the Department of Biotechnology, Govt. of India; BT/INF/22/SP17358/2016) and Central Animal Facility, IISc Bangalore are thanked for maintaining and

providing mice for this study. Sagar Tarate and Dhanashree Kelkar are thanked for technical assistance. Vineeta Bal, Satyajit Rath, Girish Deshpande, Girish Ratnaparkhi and Nishad Matange are thanked for reading and providing critical inputs to the manuscript.

Data and Materials Availability

All the data that supports the findings of this study are available in the paper (and its associated Supplementary Information) or are available from the Lead Contact on reasonable request.

References

Barnes MJ, Li CM, Xu Y, An J, Huang Y, Cyster JG. The lysophosphatidylserine receptor GPR174 constrains regulatory T cell development and function. J Exp Med. 2015; 212 :1011–20. [PubMed: 26077720]

Blankman JL, Cravatt BF. Chemical Probes of Endocannabinoid Metabolism. Pharmacological Reviews. 2013; 65 :849–871. [PubMed: 23512546]

Blankman JL, Long JZ, Trauger SA, Siuzdak G, Cravatt BF. ABHD12 controls brain lysophosphatidylserine pathways that are deregulated in a murine model of the neurodegenerative disease PHARC. Proc Natl Acad Sci U S A. 2013; 110 :1500–5. [PubMed: 23297193]

Blankman JL, Simon GM, Cravatt BF. A comprehensive profile of brain enzymes that hydrolyze the endocannabinoid 2-arachidonoylglycerol. Chem Biol. 2007; 14 :1347–56. [PubMed: 18096503]

Chimalakonda KC, Pang E, Weaver JL, Howard KE, Patel V, Boyne MT. Development and validation of a liquid-chromatography tandem mass spectrometry method to determine in vitro and in vivo histamine release. Journal of Pharmaceutical and Biomedical Analysis. 2015; 102 :494–499. [PubMed: 25459949]

Chu X, Shen M, Xie F, Miao XJ, Shou WH, Liu L, Yang PP, Bai YN, Zhang KY, Yang L, Hua Q, et al. An X chromosome-wide association analysis identifies variants in GPR174 as a risk factor for Graves' disease. J Med Genet. 2013; 50 :479–85. [PubMed: 23667180]

Contos JJA, Ishii I, Chun J. Lysophosphatidic acid receptors. Mol Pharm. 2000; 58 :1188–1196.

Dennis EA. Lipidomics In Disease And Drug Discovery. Faseb Journal. 2016; 30

Dennis EA, Norris PC. Eicosanoid storm in infection and inflammation. Nature Reviews Immunology. 2015; 15 :511–523.

Fahy E, Cotter D, Sud M, Subramaniam S. Lipid classification, structures and tools. Biochimica Et Biophysica Acta-Molecular and Cell Biology of Lipids. 2011; 1811 :637–647.

Fahy E, Subramaniam S, Brown HA, Glass CK, Merrill AH JR, Murphy RC, Raetz CR, Russell DW, Seyama Y, Shaw W, Shimizu T, et al. A comprehensive classification system for lipids. J Lipid Res. 2005; 46 :839–61. [PubMed: 15722563]

Fiskerstrand T, H'mida-Ben Brahim D, Johansson S, M'zahem A, Haukanes BI, Drouot N, Zimmermann J, Cole AJ, Vedeler C, Bredrup C, Assoum M, et al. Mutations in ABHD12 cause the neurodegenerative disease PHARC: An inborn error of endocannabinoid metabolism. Am J Hum Genet. 2010; 87 :410–7. [PubMed: 20797687]

Fiskerstrand T, Knappskog P, Majewski J, Wanders RJ, Boman H, Bindoff LA. A novel Refsum-like disorder that maps to chromosome 20. Neurology. 2009; 72 :20–27. [PubMed: 19005174]

Fowler CJ, Holt S, Nilsson O, Jonsson KO, Tiger G, Jacobsson SO. The endocannabinoid signaling system: pharmacological and therapeutic aspects. Pharmacol Biochem Behav. 2005; 81 :248–62. [PubMed: 15935456]

Frasch SC, Bratton DL. Emerging roles for lysophosphatidylserine in resolution of inflammation. Prog Lipid Res. 2012; 51 :199–207. [PubMed: 22465125]

Gardell SE, Dubin AE, Chun J. Emerging medicinal roles for lysophospholipid signaling. Trends Mol Med. 2006; 12 :65–75. [PubMed: 16406843]

Gonzalez-cabrera PJ, Brown S, Studer SM, Rosen H. S1P signaling: new therapies and opportunities. F1000Prime Rep. 2014; 6 :109. [PubMed: 25580263]

Holla S, Prakhar P, Singh V, Karnam A, Mukherjee T, Mahadik K, Parikh P, Singh A, Rajmani RS, Ramachandra SG, Balaji KN. MUSASHI-Mediated Expression of JMJD3, a H3K27me3 Demethylase, Is Involved in Foamy Macrophage Generation during Mycobacterial Infection. Plos Pathogens. 2016; 12

Hosono H, Aoki J, Nagai Y, Bandoh K, Ishida M, Taguchi R, Arai H, Inoue K. Phosphatidylserine-specific phospholipase A1 stimulates histamine release from rat peritoneal mast cells through production of 2-acyl-1-lysophosphatidylserine. J Biol Chem. 2001; 276 :29664–70. [PubMed: 11395520]

Inoue A, Ishiguro J, Kitamura H, Arima N, Okutani M, Shuto A, Higashiyama S, Ohwada T, Arai H, Makide K, Aoki J. TGFalpha shedding assay: an accurate and versatile method for detecting GPCR activation. Nat Methods. 2012; 9 :1021–9. [PubMed: 22983457]

Ishii I, Fukushima N, Ye X, Chun J. Lysophospholipid receptors: signaling and biology. Annu Rev Biochem. 2004; 73 :321–54. [PubMed: 15189145]

Iwashita M, Makide K, Nonomura T, Misumi Y, Otani Y, Ishida M, Taguchi R, Tsujimoto M, Aoki J, Arai H, Ohwada T. Synthesis and evaluation of lysophosphatidylserine analogues as inducers of mast cell degranulation. Potent activities of lysophosphatidylthreonine and its 2-deoxy derivative. J Med Chem. 2009; 52 :5837–63. [PubMed: 19743861]

Joshi A, Shaikh M, Singh S, Rajendran A, Mhetre A, Kamat SS. Biochemical characterization of the PHARC-associated serine hydrolase ABHD12 reveals its preference for very-long-chain lipids. Journal of Biological Chemistry. 2018; 293 :16953–16963.

Kamat SS, Camara K, Parsons WH, Chen DH, Dix MM, Bird TD, Howell AR, Cravatt BF. Immunomodulatory lysophosphatidylserines are regulated by ABHD16A and ABHD12 interplay. Nat Chem Biol. 2015; 11 :164–71. [PubMed: 25580854]

Kelkar DS, Ravikumar G, Mehendale N, Singh S, Joshi A, Sharma AK, Mhetre A, Rajendran A, Chakrapani H, Kamat SS. A chemical-genetic screen identifies ABHD12 as an oxidized-phosphatidylserine lipase. Nat Chem Biol. 2019; 15 :169–178. [PubMed: 30643283]

Lawson D, Fewtrell C, Raff MC. Localized mast cell degranulation induced by concanavalin A-sepharose beads. Implications for the Ca2+ hypothesis of stimulus-secretion coupling. J Cell Biol. 1978; 79 :394–400. [PubMed: 569156]

Lee SY, Lee HY, Kim SD, Jo SH, Shim JW, Lee HJ, Yun J, Bae YS. Lysophosphatidylserine stimulates chemotactic migration in U87 human glioma cells. Biochem Biophys Res Commun. 2008; 374 :147–51. [PubMed: 18616930]

Liang QL, Wu QA, Jiang JH, Duan JA, Wang C, Smith MD, Lu H, Wang Q, Nagarkatti P, Fan DP. Characterization of Sparstolonin B, a Chinese Herb-derived Compound, as a Selective Toll-like Receptor Antagonist with Potent Anti-inflammatory Properties. Journal of Biological Chemistry. 2011; 286 :26470–26479.

Liang QL, Yu F, Cui XD, Duan JA, Wu QN, Nagarkatti P, Fan DP. Sparstolonin B suppresses lipopolysaccharide-induced inflammation in human umbilical vein endothelial cells. Archives of Pharmacal Research. 2013; 36 :890–896. [PubMed: 23604718]

Lloret S, Moreno JJ. Ca2+ influx, phosphoinositide hydrolysis, and histamine release induced by lysophosphatidylserine in mast cells. J Cell Physiol. 1995; 165 :89–95. [PubMed: 7559812]

Mallik S, Prasad R, Bhattacharya A, Sen P. Synthesis of Phosphatidylserine and Its Stereoisomers: Their Role in Activation of Blood Coagulation. Acs Medicinal Chemistry Letters. 2018; 9 :434–439. [PubMed: 29795755]

Meurer SK, Ness M, Weiskirchen S, Kim P, Tag CG, Kauffmann M, Huber M, Weiskirchen R. Isolation of Mature (Peritoneum-Derived) Mast Cells and Immature (Bone Marrow-Derived) Mast Cell Precursors from Mice. Plos One. 2016; 11

Napier C, Mitchell AL, Gan E, Wilson I, Pearce SHS. Role of the X-Linked Gene GPR174 in Autoimmune Addison's Disease. Journal of Clinical Endocrinology & Metabolism. 2015; 100 :E187–E190. [PubMed: 25295623]

Napier C, Mitchell AL, Gan EH, Wilson I, Pearce SHS. Female Proclivity to Autoimmune Addison's Disease: Role of the X-Linked Gene GPR174. Endocrine Reviews. 2014; 35

Navia-Paldanius D, Savinainen JR, Laitinen JT. Biochemical and pharmacological characterization of human alpha/beta-hydrolase domain containing 6 (ABHD6) and 12 (ABHD12). J Lipid Res. 2012; 53 :2413–24. [PubMed: 22969151]

Niphakis MJ, Lum KM, Cognetta AB, 3RD, Correia BE, Ichu TA, Olucha J, Brown SJ, Kundu S, Piscitelli F, Rosen H, Cravatt BF. A Global Map of Lipid-Binding Proteins and Their Ligandability in Cells. Cell. 2015; 161 :1668–80. [PubMed: 26091042]

Ogasawara D, Ichu TA, Vartabedian VF, Benthuysen J, Jing H, Reed A, Ulanovskaya OA, Hulce JJ, Roberts A, Brown S, Rosen H, Teijaro JR, Cravatt BF. Selective blockade of the lyso-PS lipase ABHD12 stimulates immune responses in vivo. Nature Chemical Biology. 2018; 14 :1099–1108. [PubMed: 30420694]

Park KS, Lee HY, Kim MK, Shin EH, Bae YS. Lysophosphatidylserine stimulates leukemic cells but not normal leukocytes. Biochem Biophys Res Commun. 2005; 333 :353–358. [PubMed: 15946646]

Parker CG, Galmozzi A, Wang Y, Correia BE, Sasaki K, Joslyn CM, Kim AS, Cavallaro CL, Lawrence RM, Johnson SR, Narvaiza I, Saez E, Cravatt BF. Ligand and Target Discovery by Fragment-Based Screening in Human Cells. Cell. 2017; 168 :527–541 e29. [PubMed: 28111073]

Pathak D, Mehendale N, Singh S, Mallik R, Kamat SS. Lipidomics Suggests a New Role for Ceramide Synthase in Phagocytosis. ACS Chem Biol. 2018; 13 :2280–2287. [PubMed: 29963848]

Raetz CR, Whitfield C. Lipopolysaccharide endotoxins. Annu Rev Biochem. 2002; 71 :635–700. [PubMed: 12045108]

Rajendran A, Vaidya K, Mendoza J, Bridwell-Rabb J, Kamat SS. Functional Annotation of ABHD14B, an Orphan Serine Hydrolase Enzyme. Biochemistry. 2020; 59 :183–196. [PubMed: 31478652]

Rosen H, Stevens RC, Hanson M, Roberts E, Oldstone MB. Sphingosine-1-phosphate and its receptors: structure, signaling, and influence. Annu Rev Biochem. 2013; 82 :637–62. [PubMed: 23527695]

Rueden CT, Schindelin J, Hiner MC, Dezonia BE, Walter AE, Arena ET, Eliceiri KW. ImageJ2: ImageJ for the next generation of scientific image data. BMC Bioinformatics. 2017; 18 :529. [PubMed: 29187165]

Schindelin J, Rueden CT, Hiner MC, Eliceiri KW. The ImageJ ecosystem: An open platform for biomedical image analysis. Mol Reprod Dev. 2015; 82 :518–29. [PubMed: 26153368]

Shanbhag K, Mhetre A, Khandelwal N, Kamat SS. The Lysophosphatidylserines-An Emerging Class of Signalling Lysophospholipids. J Membr Biol. 2020; 253 :381–397. [PubMed: 32767057]

Singh S, Joshi A, Kamat SS. Mapping the Neuroanatomy of ABHD16A, ABHD12, and Lysophosphatidylserines Provides New Insights into the Pathophysiology of the Human Neurological Disorder PHARC. Biochemistry. 2020; 59 :2299–2311. [PubMed: 32462874]

Sugita K, Yamamura C, Tabata K, Fujita N. Expression of orphan G-protein coupled receptor GPR174 in CHO cells induced morphological changes and proliferation delay via increasing intracellular cAMP. Biochem Biophys Res Commun. 2013; 430 :190–5. [PubMed: 23178570]

Sugo T, Tachimoto H, Chikatsu T, Murakami Y, Kikukawa Y, Sato S, Kikuchi K, Nagi T, Harada M, Ogi K, Ebisawa M, Mori M. Identification of a lysophosphatidylserine receptor on mast cells. Biochem Biophys Res Commun. 2006; 341 :1078–87. [PubMed: 16460680]

Sullivan TJ, Greene WC, Parker CW. Concanavalin A-induced histamine release from normal rat mast cells. J Immunol. 1975; 115 :278–82. [PubMed: 50352]

Szymanski K, Miskiewicz P, Pirko K, Jurecka-Lubieniecka B, Kula D, Hasse-Lazar K, Krajewski P, Bednarczuk T, Ploski R. rs3827440, a nonsynonymous single nucleotide polymorphism within GPR174 gene in X chromosome, is associated with Graves' disease in Polish Caucasian population. Tissue Antigens. 2014; 83 :41–4. [PubMed: 24289805]

Tracey TJ, Steyn FJ, Wolvetang EJ, Ngo ST. Neuronal Lipid Metabolism: Multiple Pathways Driving Functional Outcomes in Health and Disease. Frontiers in Molecular Neuroscience. 2018; 11

Van Der Kleij D, Latz E, Brouwers JF, Kruize YC, Schmitz M, Kurt-Jones EA, Espevik T, De Jong EC, Kapsenberg ML, Golenbock DT, Tielens AG, Yazdanbakhsh M. A novel host-parasite lipid cross-talk. Schistosomal lyso-phosphatidylserine activates toll-like receptor 2 and affects immune polarization. J Biol Chem. 2002; 277 :48122–9. [PubMed: 12359728]

Vance JE. Phospholipid Synthesis and Transport in Mammalian Cells. Traffic. 2015; 16 :1–18. [PubMed: 25243850]

Wu C, Jin X, Tsueng G, Afrasiabi C, Su AI. BioGPS: building your own mash-up of gene annotations and expression profiles. Nucleic Acids Res. 2016; 44 :D313–6. [PubMed: 26578587]

Wymann MP, Schneiter R. Lipid signalling in disease. Nature Reviews Molecular Cell Biology. 2008; 9 :162–176. [PubMed: 18216772]

Yanagida K, Valentine WJ. Druggable Lysophospholipid Signaling Pathways. Adv Exp Med Biol. 2020; 1274 :137–176. [PubMed: 32894510]

Europe PMC Funders Author Manuscripts

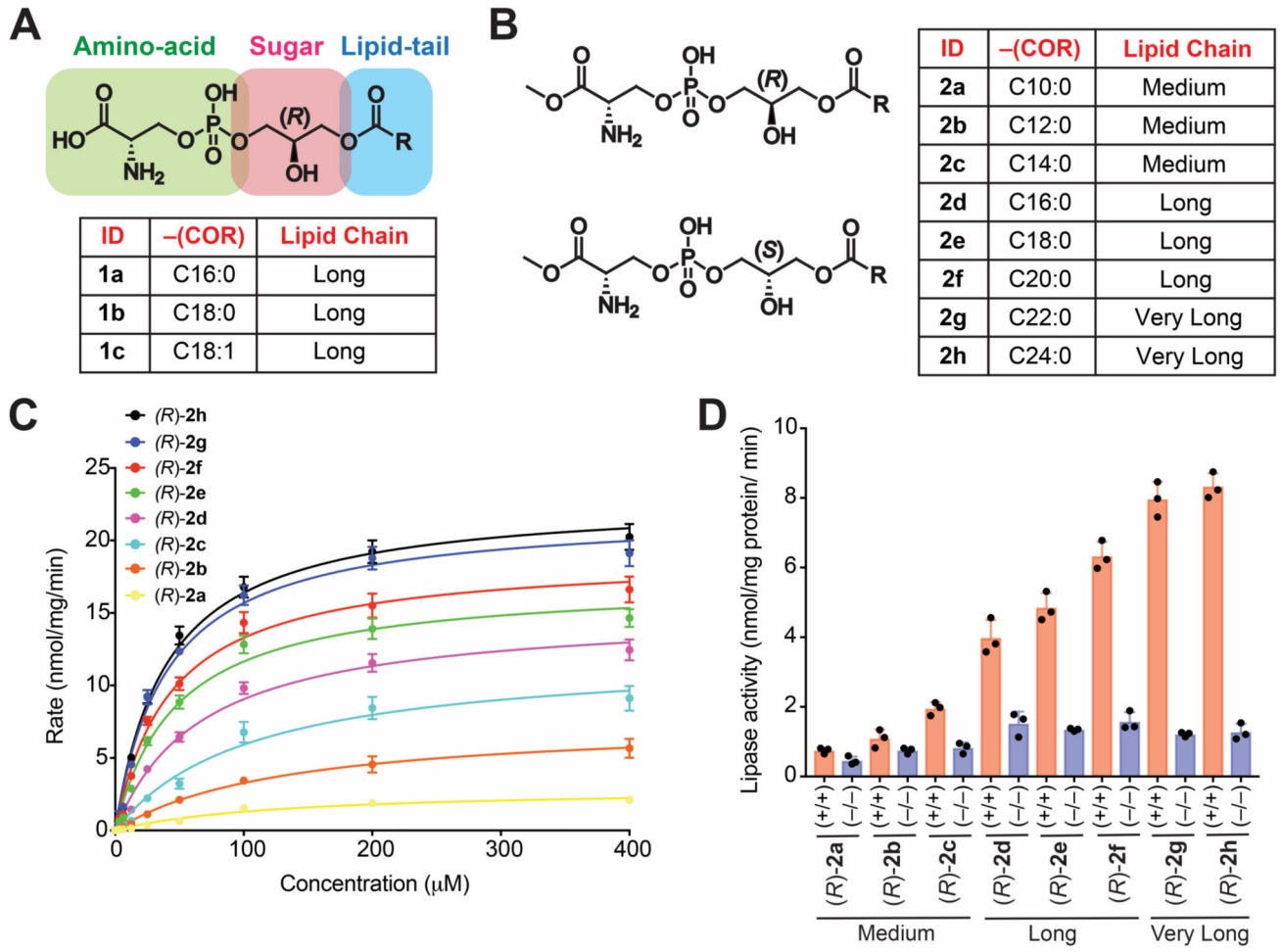

ID	–(COR)	Lipid Chain
1a	C16:0	Long
1b	C18:0	Long
1c	C18:1	Long

ID	–(COR)	Lipid Chain
2a	C10:0	Medium
2b	C12:0	Medium
2c	C14:0	Medium
2d	C16:0	Long
2e	C18:0	Long
2f	C20:0	Long
2g	C22:0	Very Long
2h	C24:0	Very Long

Figure 1. Structure of Me-lyso-PSs, and testing them as substrates against ABHD12.

The chemical structures of (**A**) commercially available canonical natural lyso-PSs and (**B**) our synthetic Me-lyso-PS lipid library with both (*R*)- and (*S*)-stereoisomers. (**C**) Enzyme kinetic assays for membrane lysates (10 μg) of HEK293T cells transfected with hABHD12 tested against the (*R*)-Me-lyso-PSs (0 – 400 μM, 30 mins, 37 °C, n = 3/data point). The line connecting the points, represents a fit to the Michaelis-Menten enzyme kinetics equation. See Table 1 for all enzyme kinetics parameters. (**D**) Lipase assays for (*R*)-Me-lyso-PSs (100 μM, 30 mins, 37 °C, n = 3/group) tested against brain membrane lysates (20 μg) from wild type (+/+) or ABHD12 knockout (–/–) mice. All data presented in (**C**, data points), and (**D**, bars) is represented as mean ± standard deviation.

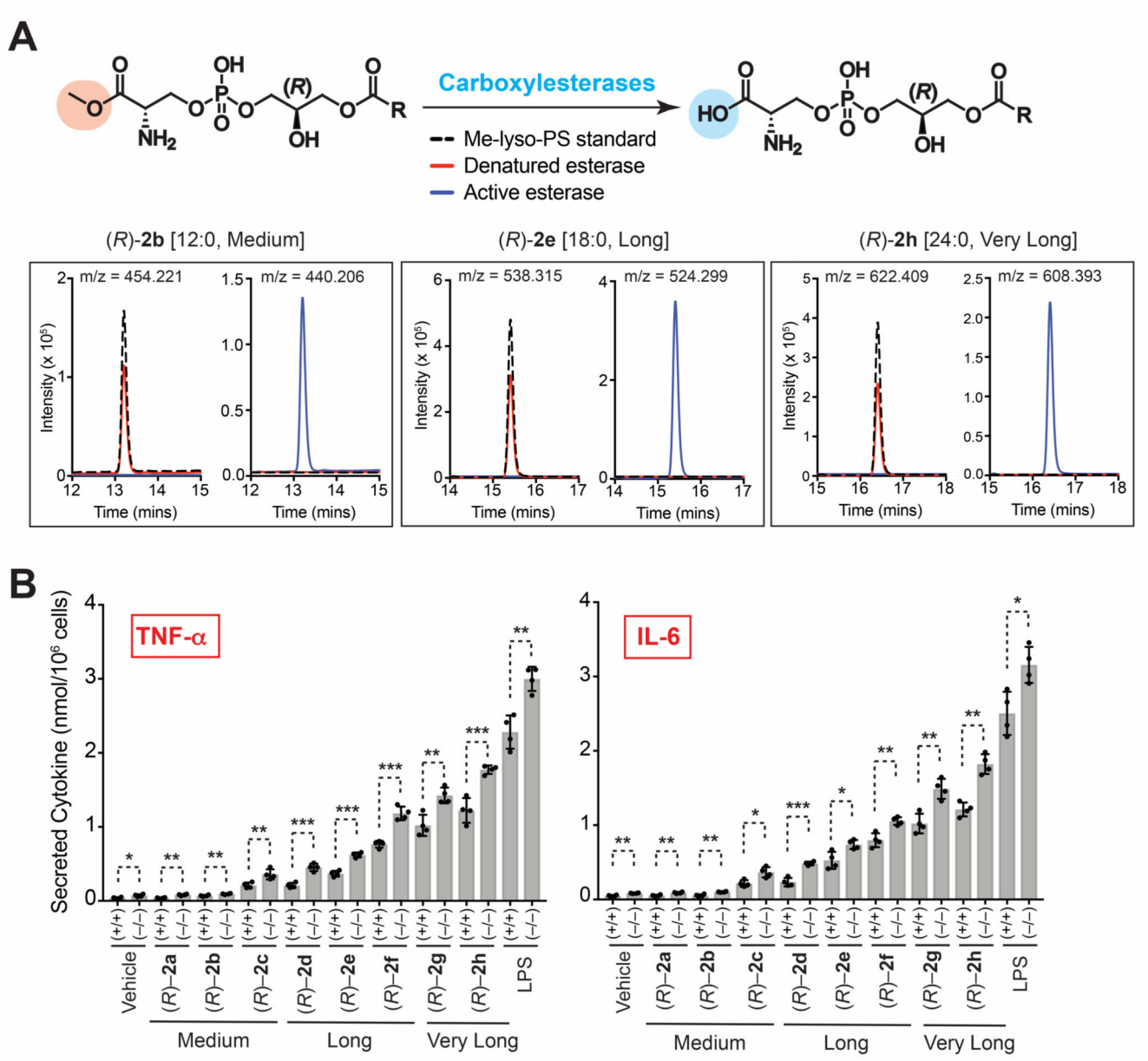

Figure 2. Metabolism of Me-lyso-PSs by carboxylesterases and the pro-inflammatory activity of Me-lyso-PSs in macrophages.

(**A**) *Top*: The enzymatic reaction for metabolism (hydrolysis) of Me-lyso-PSs to the corresponding lyso-PSs catalyzed by carboxylesterases; *Bottom*: Extracted ion chromatograms from a LC-MS analysis of (*R*)-**2b** (C12:0) ($[M-H]^-$ = 454.221), (*R*)-**2e** (C18:0) ($[M-H]^-$ = 538.315) and (*R*)-**2h** (C24:0) ($[M-H]^-$ = 622.409) showing the complete conversion of the parent compound (Me-lyso-PS) to the corresponding lyso-PS (loss of 14 Da) following treatment with active (blue trace), but not denatured (red trace), porcine liver carboxylesterase (0.1 U, 15 mins, 37 °C). In these assays, 100 械 g of the (*R*)-Me-lyso-PS was used, and a no-enzyme standard only control (dotted black trace) was also included for the same treatment. This LC-MS experiment was done twice for each of the (*R*)-Me-lyso-

PS, with reproducible result each time. (**B**) Secreted TNF-α and IL-6 from PPM harvested from wild type (+/+) or ABHD12 knockout (–/–) mice following treatment with vehicle (DMSO) or lipopolysaccharide (LPS) or (*R*)-**2a-h** (1 械 M, 4 hours, 37 °C); *p < 0.05, **p < 0.01, and ***p < 0.001 versus (+/+) group by Student's two-tailed *t*-test.

Europe PMC Funders Author Manuscripts

Europe PMC Funders Author Manuscripts

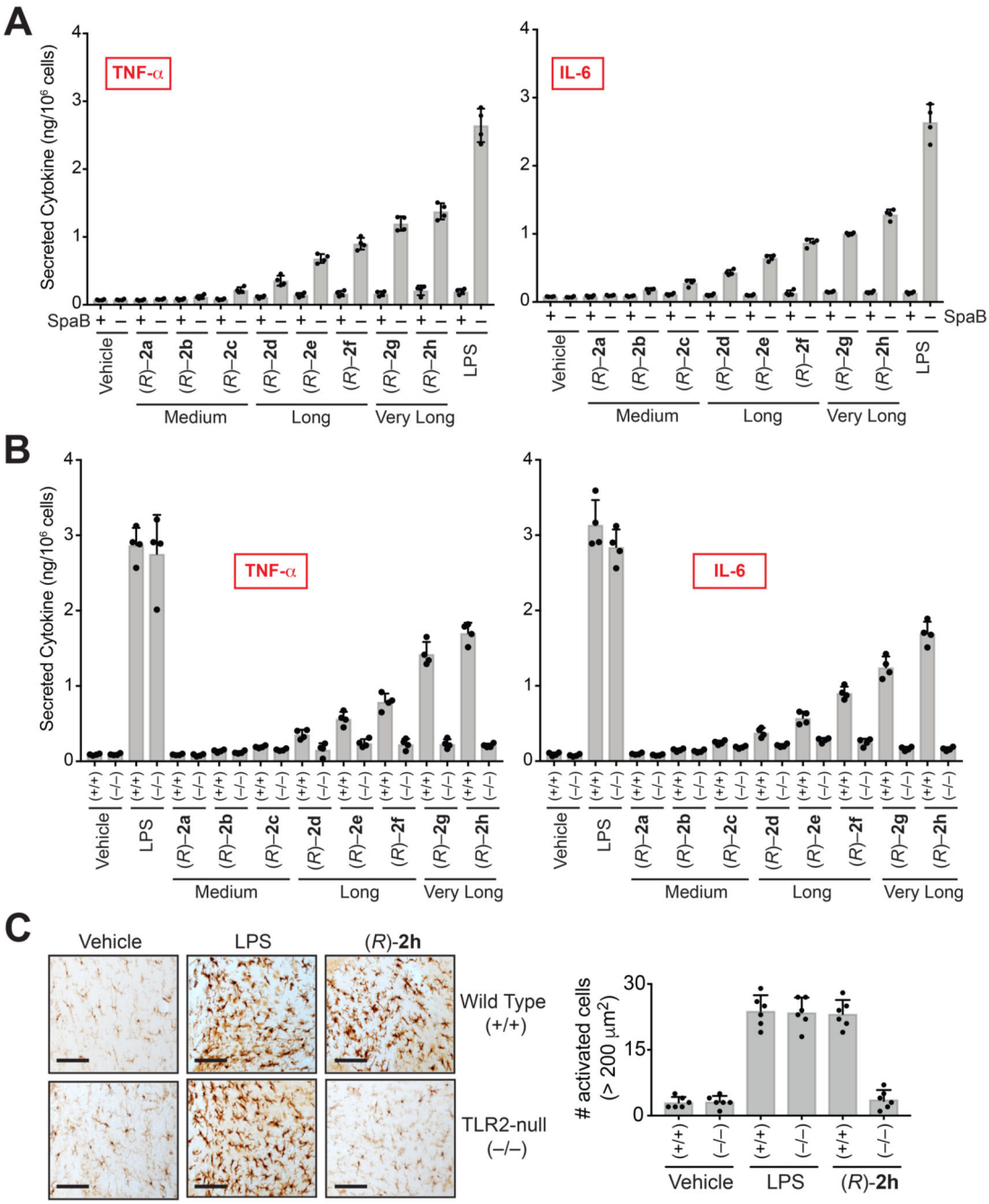

Figure 3. VLC lyso-PSs elicit pro-inflammatory responses via a TLR2 dependent pathway.

Secreted TNF-α and IL-6 from PPM harvested from (**A**) wild type mice pre-treated with DMSO or SpaB (10 μM, 4 hours, 37 °C), followed by treatment with vehicle or LPS or (*R*)-**2a-h** (1 μM, 4 hours, 37 °C); (**B**) wild type (+/+) or TLR2 knockout (–/–) mice following treatment with vehicle or LPS or VLC (*R*)-Me-lyso-PSs (1 μM, 4 hours, 37 °C). (**C**) Representative images from Iba-1 immunostaining for microglial activation (black bar = 250 μm) and quantification of enlarged cells (>200 μm^2) in the cerebellum (per 1.44 mm^2) of wild type (+/+) or TLR2 knockout (–/–) mice following intravenous injection

of vehicle (PBS), LPS or (*R*)-**2h** (C24:0) (all 1 mg/kg body weight, 10 hours). All data presented in (**A**), (**B**), and (**C**) is represented as mean ± standard deviation (n = 4-6/group).

Europe PMC Funders Author Manuscripts

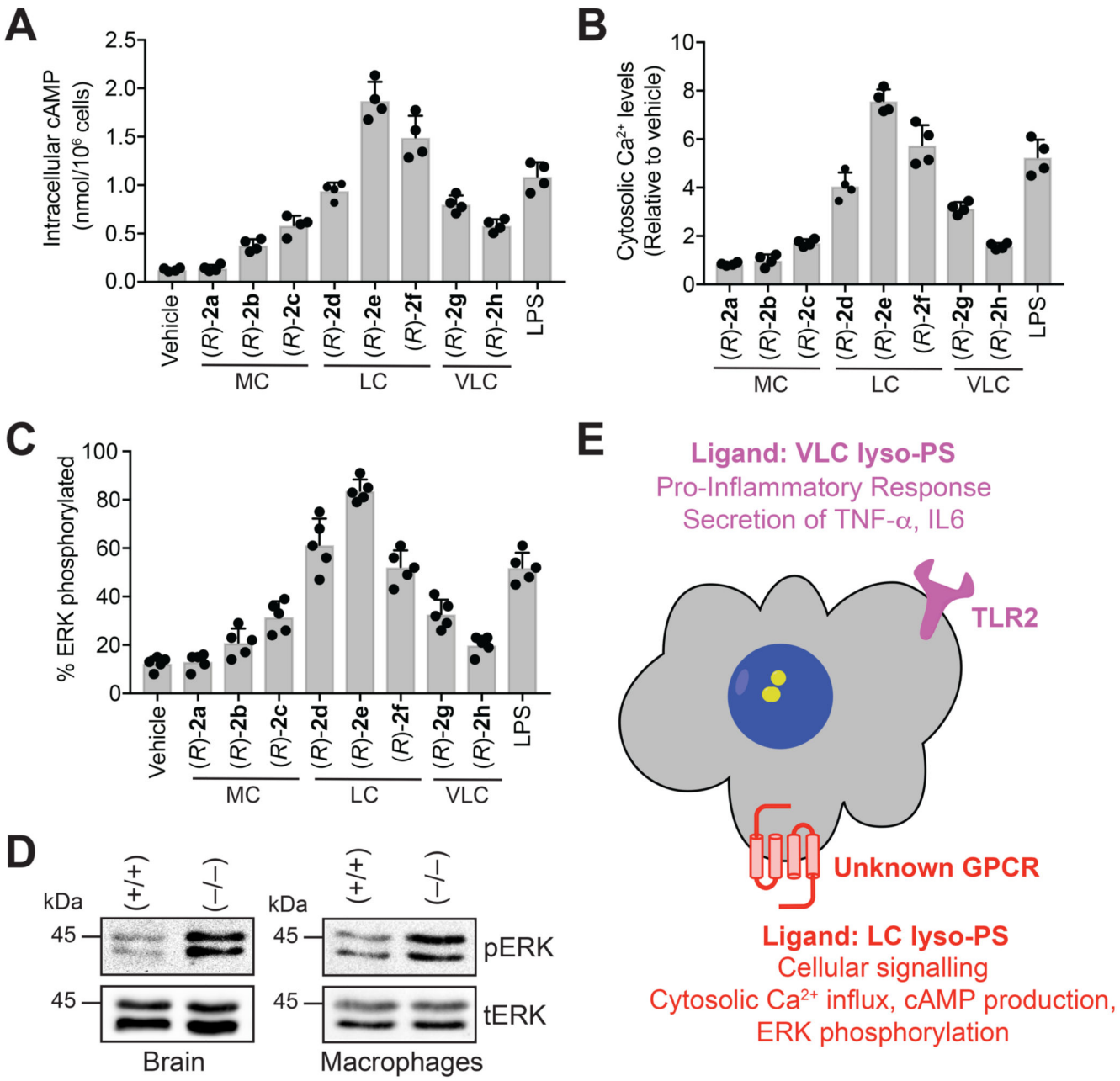

Figure 4. LC lyso-PSs activate macrophages through a putative GPCR.

(**A**) Intracellular cAMP, (**B**) relative cytosolic Ca^{2+} levels, and (**C**) percentage of phosphorylated ERK from WT PPM following treatment with vehicle (DMSO) or LPS or (*R*)-**2a-h** (1 μM, 10 mins, 37 °C). All data presented in (**A**), (**B**), and (**C**) is represented as mean ± standard deviation (n = 4-5/group), where MC = medium chain, LC = long chain and VLC = very-long chain. (**D**) Representative western blots on lysates of brain (6-month-old mice) and LPS-treated (1 μM, 4 hours, 37 °C) PPM harvested from wild type (+/+) or ABHD12-null (–/–) mice, showing enhanced phosphorylation of ERK in both these tissues

for the ABHD12-null (–/–) genotype. (**E**) Schematic cartoon representation summarizing the lyso-PS signaling pathways by possibly two types of receptors on mammalian macrophages.

Europe PMC Funders Author Manuscripts

Europe PMC Funders Author Manuscripts

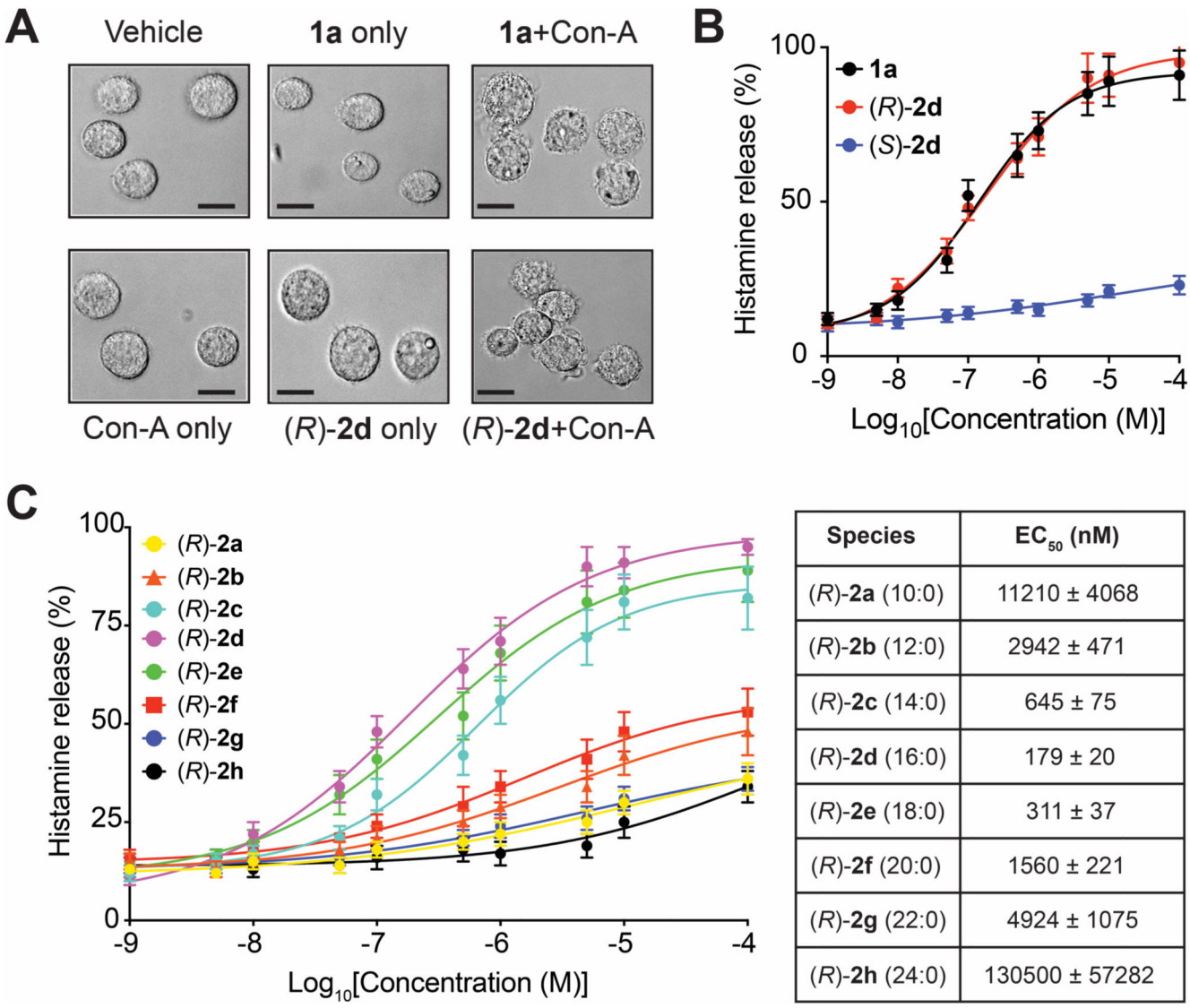

Species	EC_{50} (nM)
(*R*)-**2a** (10:0)	11210 ± 4068
(*R*)-**2b** (12:0)	2942 ± 471
(*R*)-**2c** (14:0)	645 ± 75
(*R*)-**2d** (16:0)	179 ± 20
(*R*)-**2e** (18:0)	311 ± 37
(*R*)-**2f** (20:0)	1560 ± 221
(*R*)-**2g** (22:0)	4924 ± 1075
(*R*)-**2h** (24:0)	130500 ± 57282

Figure 5. LC lyso-PSs robustly cause histamine release from primary mast cells.

(**A**) Representative microscopy image showing degranulation of PCMCs after **1a** (C16:0 lyso-PS) or (*R*)-**2d** (C16:0) treatment (both 1 械 M, 30 mins, 37 °C) in the presence of concanavalin A (Con-A) (black bar = 100 械 m). (**B**) Histamine release profile from PCMCs treated with **1a** (C16:0 lyso-PS) or (*R*)-**2d** (C16:0) or (*S*)-**2d** (C16:0) (1 nM to 10 mM, 30 mins, 37 °C, n = 3/data point). (**C**) Dose response and EC_{50} values for histamine release from PCMCs following treatment with the different (*R*)-Me-lyso-PSs (1 nM to 10 mM, 30 mins, 37 °C, n = 3/data point).

Europe PMC Funders Author Manuscripts

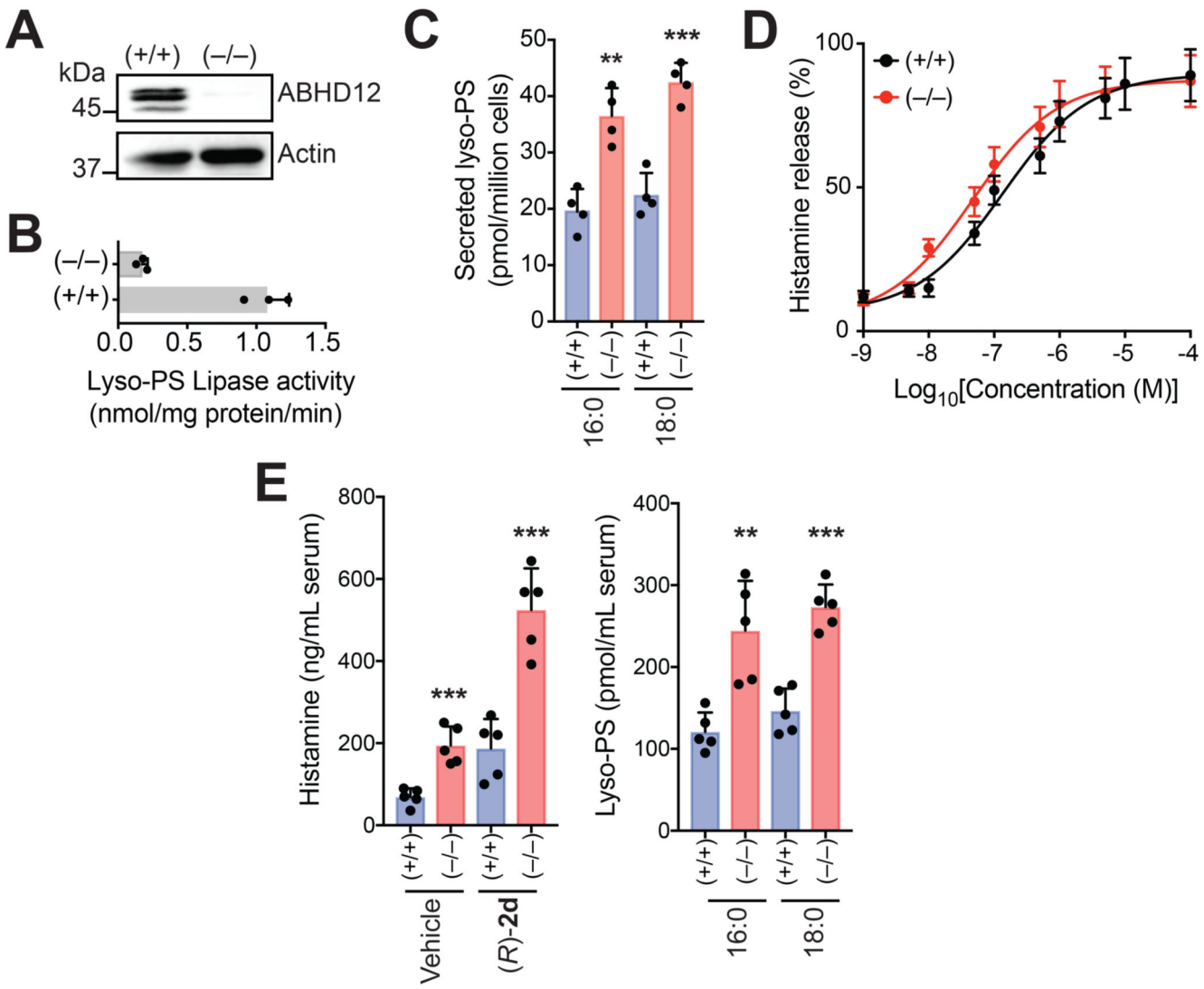

Figure 6. ABHD12 controls concentrations of LC lyso-PSs in primary mast cells, and thereby serum histamine levels.

(**A**) Representative western blot and (**B**) lyso-PS lipase activity assay (100 械 M **1a** (C16:0 lyso-PS), 30 mins, 37 °C, n = 3/group), showing the loss of ABHD12 in PCMCs derived from ABHD12 knockout (–/–) mice. (**C**) Concentrations of lyso-PS secreted from cultured PCMCs derived from wild type (+/+) or ABHD12 knockout (–/–) mice, showing significantly increased **1a** (C16:0 lyso-PS) and **1b** (C18:0 lyso-PS) secretion from ABHD12-null PCMCs (n = 4/group). (**D**) Histamine release profiles from PCMCs derived from wild type (+/+) or ABHD12 knockout (–/–) mice treated with **1a** (C16:0 lyso-PS) (1 nM to 10 mM, 30 mins, 37 °C, n = 3/data point). **(E)** *Left*, Serum histamine levels in (+/+) or (–/–) mice following intravenous injections with vehicle (PBS) or (*R*)-**2d** (C16:0) (1 mg/kg, 2 hours), showing increased serum histamine concentrations in the (–/–) mice compared to (+/+) controls for both treatments (n = 5/group). Interestingly, systemic administration of (*R*)-**2d** (C16:0) in (+/+) mice, produces significantly more circulating serum histamine compared to the vehicle group, showing that (*R*)-**2d** (C16:0) by itself can induce histamine

release from mast cells in *in vivo* settings. *Right*, Serum lyso-PS concentrations in (+/+) or (–/–) mice, showing increased concentrations of circulating **1a** (C16:0 lyso-PS) and **1b** (C18:0 lyso-PS) in (–/–) mice, corroborating the increased serum histamine levels seen in these mice (n = 5/group). All data presented in this figure is represented as mean ± standard deviation from at least n independent experiments. **p < 0.01, and ***p < 0.001 versus (+/+) group by Student's two-tailed *t*-test.

Europe PMC Funders Author Manuscripts

Table 1

Kinetic constants for lyso-PS and Me-lyso-PS substrates tested against hABHD12 (HEK293T membrane lysates transiently transfected with hABHD12).

Lyso-PS species	Fatty acid chain length: unsaturation	V_{max} (nmol/mg protein/min)	K_M (μM)	V_{max}/K_M (nmol/mg protein/min/M) (x 10^5)
1a	16:0	15.6 ± 0.6	72 ± 8	2.2 ± 0.3
1b	18:0	18.3 ± 0.5	48 ± 4	3.8 ± 0.4
1c	18:1	17.8 ± 0.6	46 ± 6	3.8 ± 0.5
(*R*)-**2a**	10:0	2.9 ± 0.2	126 ± 18	0.2 ± 0.04
(*R*)-**2b**	12:0	7.6 ± 0.3	131 ± 14	0.6 ± 0.06
(*R*)-**2c**	14:0	12.2 ± 0.6	106 ± 14	1.1 ± 0.1
(*R*)-**2d**	16:0	15.2 ± 0.6	67 ± 7	2.3 ± 0.3
(*R*)-**2e**	18:0	17.2 ± 0.6	47 ± 5	3.7 ± 0.5
(*R*)-**2f**	20:0	19.0 ± 0.6	43 ± 4	4.4 ± 0.5
(*R*)-**2g**	22:0	22.0 ± 0.6	40 ± 4	5.5 ± 0.6
(*R*)-**2h**	24:0	22.9 ± 0.6	40 ± 4	5.7 ± 0.6
(*S*)-**2a**	10:0	0.2 ± 0.02	275 ± 32	0.007 ± 0.001
(*S*)-**2b**	12:0	0.4 ± 0.05	255 ± 35	0.016 ± 0.002
(*S*)-**2c**	14:0	0.6 ± 0.1	215 ± 28	0.028 ± 0.003
(*S*)-**2d**	16:0	0.8 ± 0.1	187 ± 24	0.043 ± 0.006
(*S*)-**2e**	18:0	1.2 ± 0.1	178 ± 25	0.067 ± 0.008
(*S*)-**2f**	20:0	1.3 ± 0.2	165 ± 23	0.078 ± 0.009
(*S*)-**2g**	22:0	1.2 ± 0.2	167 ± 26	0.072 ± 0.009
(*S*)-**2h**	24:0	1.2 ± 0.3	176 ± 31	0.068 ± 0.008